Department of Applied Physics

Photolithographic fabrication of periodic nanostructures for photonic applications

Aleksandr Kravchenko

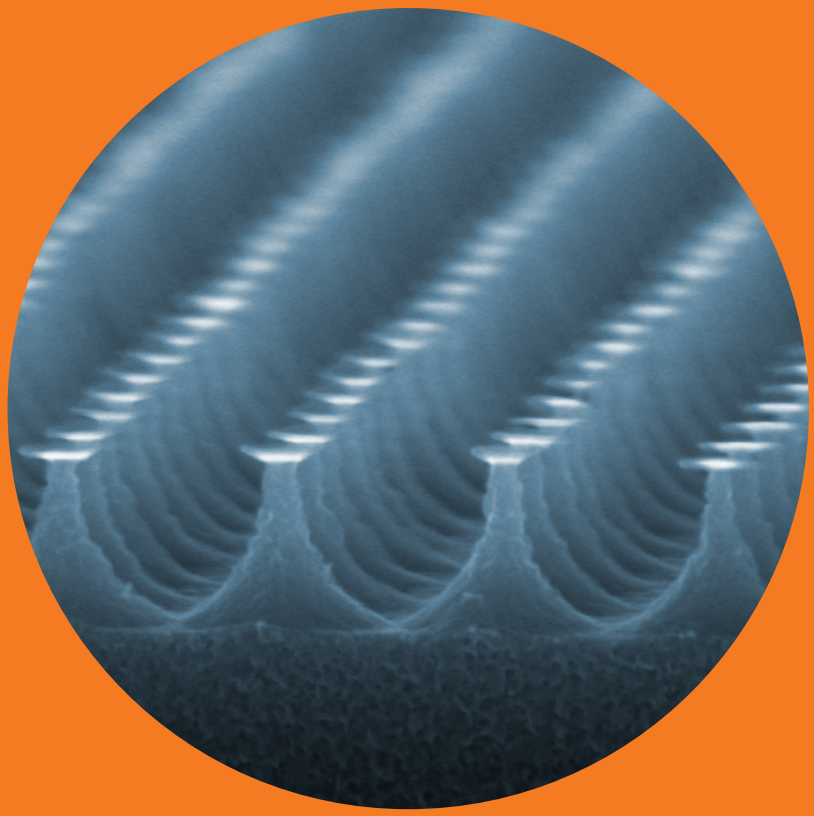

Aalto University

DOCTORAL DISSERTATIONS

Aalto University publication series
DOCTORAL DISSERTATIONS 116/2015

Photolithographic fabrication of periodic nanostructures for photonic applications

Aleksandr Kravchenko

A doctoral dissertation completed for the degree of Doctor of Science (Technology) to be defended, with the permission of the Aalto University School of Science, at a public examination held at the lecture hall AS1 of the TUAS building (Otaniementie 17, Espoo, Finland) on the 27th of November 2015 at 13.

Aalto University
School of Science
Department of Applied Physics
Optics and Photonics group

Supervising professor
Prof. Matti Kaivola

Thesis advisor
Dr. Andriy Shevchenko

Preliminary examiners
Prof. Stefan Linden, Universität Bonn, Germany
Prof. Jani Tervo, University of Eastern Finland, Finland

Opponent
Assoc. Prof. Alexander Dmitriev, Chalmers University of Technology, Sweden

Aalto University publication series
DOCTORAL DISSERTATIONS 116/2015

ISBN 978-952-60-6336-2 (printed)
ISBN 978-952-60-6337-9 (pdf)
ISSN-L 1799-4934
ISSN 1799-4934 (printed)
ISSN 1799-4942 (pdf)
http://urn.fi/URN:ISBN:978-952-60-6337-9

Unigrafia Oy
Helsinki 2015

Finland

Author
Aleksandr Kravchenko

Name of the doctoral dissertation
Photolithographic fabrication of periodic nanostructures for photonic applications

Publisher School of Science

Unit Department of Applied Physics

Series Aalto University publication series DOCTORAL DISSERTATIONS 116/2015

Field of research Engineering Physics

Manuscript submitted 14 April 2015 **Date of the defence** 27 November 2015

Permission to publish granted (date) 23 June 2015 **Language** English

☐ **Monograph** ☒ **Article dissertation (summary + original articles)**

Abstract

Artificial micro- and nanostructures have already found numerous applications in various sectors of optics and photonics. Periodic patterns are used as diffraction gratings, photonic crystals, ultrathin polarizers and wave retarders, antireflection coatings, optical filters, plasmonic waveguides, optical antennas and sensors, as well as substrates for surface enhanced fluorescence and Raman spectroscopy (SERS). Surface micro- and nanostructures have also been demonstrated to exhibit superhydro- and superoleophobicity and, for example, the so-called structural colors that do not use any dyes. These properties can lead to fascinating applications, e.g., in self-cleaning eyeglasses and touchscreens, as well as in various types of displays.

This thesis describes the development of a set of nanofabrication techniques for manufacturing nanoscale optical components. One of the key ideas was to switch from conventional photolithography based on photoresist to a new type of maskless lithography making use of azobenzene-containing polymers (azo-polymers). This transition fundamentally changes the fabrication process, for example, eliminating wet processing steps, such as photoresist development and stripping. The azo-polymer-based interference lithography developed in this thesis is a fast and simple technique to pattern large-area arrays of perfectly ordered nanofeatures. In addition, the azo-polymers are insensitive to humidity and temperature fluctuations, as well as to stray light. These properties make them an attractive alternative to traditional photoresists.

The invented nanofabrication technique was shown to be capable of patterning various materials, such as semiconductors, glass and metals. Using the technique we have fabricated various optical elements, such as plasmonic filters, ultrathin polarizers, all-metal reflective waveplates and substrates for surface enhanced Raman scattering with various degree of complexity. Maskless lithography allows for fast adjustment of the pattern parameters and nearly instant prototyping. The scaling up capability of the technique, meanwhile, opens up the door to industrial applications.

Keywords Azo-polymers, lithography, nanopatterning, plasmonics

ISBN (printed) 978-952-60-6336-2 **ISBN (pdf)** 978-952-60-6337-9

ISSN-L 1799-4934 **ISSN (printed)** 1799-4934 **ISSN (pdf)** 1799-4942

Location of publisher Helsinki **Location of printing** Helsinki **Year** 2015

Pages 95 **urn** http://urn.fi/URN:ISBN:978-952-60-6337-9

Preface

How many blissful revelations
The spirit of enlightment hides!
And then experience born of lapses
And genius antinomy-wise
And chance, the heavenly inventor...

A. S. Pushkin, approx. Nov. – Dec. 1829.
First published – “Russkaja Starina”, November 1884, p. 349.

The research work summarized in this thesis has been carried out in the Optics and Photonics group at the Department of Applied Physics of Aalto University (former Helsinki University of Technology). I would never have got this far without the help of dozens of people I met throughout my studies and I am very grateful to all of them.

I am very grateful to my supervisor Prof., Dr. Matti Kaivola and my advisor Docent, Dr. Andriy Shevchenko who accepted me for the graduate studies and guided my academic progress for four years. I am extremely grateful to Dr. Victor Ovchinnikov from Aalto Nanofab - the most knowledgeable expert in nanofabrication I have ever met who helped me to solve a multitude of technological mysteries. Special thanks go to Prof., Dr. Arri Priimagi who guided me through the labyrinths of polymer chemistry, inspired new ideas and supported the development of our laboratory.

This dissertation is the final step in over 20 years of my education. I am outmost grateful to my parents for planting in me an obsession with the technology and an infinite support from the very beginning. Special thanks go to Nayla Samsonova for being my teacher of electronics for over 6 years. I am very thankful to Prof., Dr. Valery Sysun, Prof., Dr. Anatoly Khakhaev, Lidia Luizova and Aleksey Moschevikin, all from Petrozavodsk State University (PetrSU), for guiding me through my bachelor studies

and opening a window to the fascinating science of Optics. Also many other people from PetrSu supported me as a beginning scientist: Dmitry Balashov, Artem Bulba, bros. Konstantin and Dmitry Ekomov, Natalia Ershova, Sergei Kiprushkin, Aleksandr Pergament, Sergei Podrjadchikov, Aleksei Solovev, Aleksei Shtykov, Aleksandr Galov, Olga Koenen, Irina Nekrylova, Igor Shibaev, Aleksandr Scherbina, Valery Gostev, and Sergey Kurskov.

I am very grateful to those, who made possible my studies at Royal Institute of Technology (KTH): Urban Westergren and Eva Andersson for accepting me to the MSc programme "Photonics" as well as the Swedish Institute and especially Michael Skoglund for providing financial support for those studies. I direct many thanks to Prof., Dr. Sergei Popov from KTH and Dr. Qin Wang from Acreo AB for being fantastic academic supervisors and simply for sharing vital life experience in a new country. I also want to express my gratitude to Dr. Lin Dong, Dr. Andrea Pinnos, Dr. Vytautas Liuolia, Dr. Dmitry Dzibrou, Dr. Kristinn Gylfason, Dr. Zhenzhong Zhang and to Sven Valerio.

Further advance of my research would have been impossible without the support from many colleagues and friends at Aalto University. I want to express my gratitude to my colleagues for contributing to my research: Patrick Grahn and Roman Khakimov for their valuable help with theoretical calculations and numerical simulations; Robert Moerland, Jenni Koskela, Mikael Simberg and Stefan van der Vegte for the amazing research that led to Publication IV. Many thanks go to Prof., Dr. Robin Ras for fruitful discussions on nanopatterned surfaces. I am very grateful to Dr. Veli-Matti Airaksinen, Paula Hekkila, Paula Kettula and Risro Salo for their efforts in running Micronova cleanroom and laboratories. I express my warm thanks to all those people who took care of the scientific equipment and made the smooth progresss of the experiments possible.

I also thank Ville Pale, Mikko Ruoho, Ismo Heikkinen, Juha Luotio, Miikka Mannisto, Igor Shavrin, Alexander Saveley, Vitaly Emets, Andrey Timofeev, Alexander Popkov and Lur Eguiluz for wonderful and relaxing moments we have shared during the years.

The funding of this work has been provided by the Academy of Finland (Projects 134029, 135106 and 135106). The cleanroom facilities were provided by Micronova Nanofabrication Centre of Aalto University.

Espoo, August 25, 2015,

Aleksandr Kravchenko

Contents

List of Publications

This thesis consists of an overview and of the following publications which are referred to in the text by their Roman numerals.

I A. Kravchenko, A. Shevchenko, V. Ovchinnikov, A. Priimagi, and M. Kaivola. Optical Interference Lithography Using Azobenzene-Functionalized Polymers for Micro- and Nanopatterning of Silicon. *Advanced Materials*, **23**, 4174-4177, 2011.

II A. Kravchenko, A. Shevchenko, P. Grahn, V. Ovchinnikov, and M. Kaivola. Photolithographic periodic patterning of gold using azobenzene-functionalized polymers. *Thin Solid Films*, **540**, 162-167, 2013.

III A. Kravchenko, A. Shevchenko, V. Ovchinnikov, P. Grahn, and M. Kaivola. Fabrication and characterization of a large-area metal nanogrid wave plate. *Applied Physics Letters*, **103**, 033111, 2013.

IV R. J. Moerland, J. E. Koskela, A. Kravchenko, M. Simberg, S. van der Vegte, M. Kaivola, A. Priimagi, and R. H. A. Ras. Large-area arrays of three-dimensional plasmonic subwavelength-sized structures from azopolymer surface-relief gratings. *Materials Horizons*, **1**, 74-80, 2014.

Author's Contribution

Publication I: "Optical Interference Lithography Using Azobenzene-Functionalized Polymers for Micro- and Nanopatterning of Silicon"

The author developed the nanofabrication technology based on a theoretical concept proposed by A. Shevchenko, and fabricated samples under the supervision of A. Shevchenko and V. Ovchinnikov. The author participated in the analysis of the results and writing of the manuscript.

Publication II: "Photolithographic periodic patterning of gold using azobenzene-functionalized polymers"

The author developed all the nanofabrication steps for the technique, fabricated the samples and performed optical measurements. The author also participated in the analysis of the results and in writing the paper.

Publication III: "Fabrication and characterization of a large-area metal nano-grid wave plate"

The author invented the use of alumina and chlorotrimethylsilane to separate metal from the silicon template. In addition, the author performed all the optical measurements together with A. Shevchenko, participated in the analysis of the experimental results and in writing the paper.

Publication IV: "Large-area arrays of three-dimensional plasmonic subwavelength-sized structures from azopolymer surface-relief gratings"

The author did metal evaporation onto the samples and specimen imaging using a scanning electron microscope. He also participated in scientific discussions and analysis of the obtained results.

1. Introduction

The recent progress in studying light-matter interaction on the micrometer and nanometer scale in parallel with developments in techniques to fabricate complex nanostructures has made micro- and nanophotonics a highly topical area of research. In particular, optical resonances that can be excited in metal and dielectric nanostructures have been very actively studied. Plasmon or Mie-type resonant excitations in individual nanoparticles are accompanied by a significant enhancement of optical scattering and absorption by the particles around the resonance wavelength. This can be used to efficiently control light propagation characteristics in nanoparticle arrays. Furthermore, the strength of the optical electric field can be significantly enhanced close to the nanostructure in which a resonant plasmon is excited. This can be used, e.g., in surface enhanced Raman spectroscopy (SERS). Also by making use of non-resonant interaction of light with periodic micro- and nanostructures, it is possible to create a variety of optical elements, such as nanogratings, spectral filters, polarizers, wave retarders, lenses, and other elements with a thickness that is smaller than the wavelength of light.

Direct fabrication of periodic nanoparticle arrays with non-trivial geometries is not a straightforward process. Usually such elements are fabricated by combining conventional photolithography with more sophisticated nanofabrication techniques. The main difficulties arise from several unwanted physical and chemical effects. Standing-wave formation in photolithographic exposure patterns drastically degrades the photoresist mask quality, when the exposure is done on a reflective substrate. Photoresist itself is very sensitive to temperature and humidity variations as well as to stray light, which leads to the requirement of carefully controlling the environment. Etching the substrate through a photoresist mask can be inefficient, when a hard substrate material, such as glass, is used.

Dry etching of noble metals is commonly considered to be impossible due to a lack of volatile noble-metal-based compounds.

An alternative nanofabrication technique is introduced in this thesis. The technique uses special photosensitive azobenzene-containing polymers (azo-polymers). In contrast to photoresists, these polymers are sensitive to light polarization rather than intensity, which in particular removes the stray-light problem and substantially reduces the influence of the standing waves on the exposure-pattern formation. In addition, azo-polymers are insensitive to temperature and humidity fluctuations, and have much longer shelf lifetimes. It is also important that azo-polymers allow one to use all-dry fabrication procedures, which greatly improves the manufacturing throughput.

Chapter 2 of this thesis describes the principles and key properties of some relevant nanofabricated optical elements. The details of the developed new nanofabrication approach are described in chapters 3 and 4 which are based on Publications I - IV. These chapters describe the fundamentals of the azo-polymer based interference lithography, the nanofabrication processes used to manufacture the various ultrathin optical components and the extension of the method towards patterning metal films and glass substrates. Chapter 4 introduces photonic structures fabricated by using the developed nanofabrication techniques. The last chapter 5 summarizes the results obtained in the thesis.

2. Periodic structures for photonic applications

Artificial micro- and nanostructures are nowadays widely used in various aspects of the daily life, technology and science. The versatility of micro- and nanostructured films is reflected in numerous applications in optics, where they have been used, e.g., to fabricate diffraction gratings [1], photonic crystals [2, 3, 4, 5, 6], ultrathin polarizers [7] and wave retarders [8, 9], antireflection (AR) coatings [10], optical filters [11], plasmonic waveguides [12], optical antennas or sensors [13], as well as substrates for surface enhanced Raman spectroscopy (SERS) [14]. Surface micro- and nanostructures can have other fascinating physical properties, exhibiting, e.g., super hydro- and oleophobicity [15, 16, 17] and so-salled structural colors that do not use any dyes [18]. This section describes these optical elements in some detail.

2.1 Diffraction gratings

A periodic array of diffracting elements capable of splitting a light beam into several beams is called diffraction grating. The simplest grating is a *transmissive amplitude grating* that is made of repeating slits in an opaque screen [1]. It is schematically shown in Fig. 2.1. When a plane wave is let through the grating, at some incidence angle θ_i, each slit acts as a source of an optical wave that diverges perpendicularly to the slit. The waves overlap and for some propagation directions interfere constructively. These directions are the directions of the diffraction orders of the grating. An optical beam incident onto the grating at an angle θ_i will thus be split into several beams corresponding to these orders. The diffraction angles θ_m of each order m can be calculated using the *grating equation*

$$a\,(sin\theta_m - sin\theta_i) = m\lambda \tag{2.1}$$

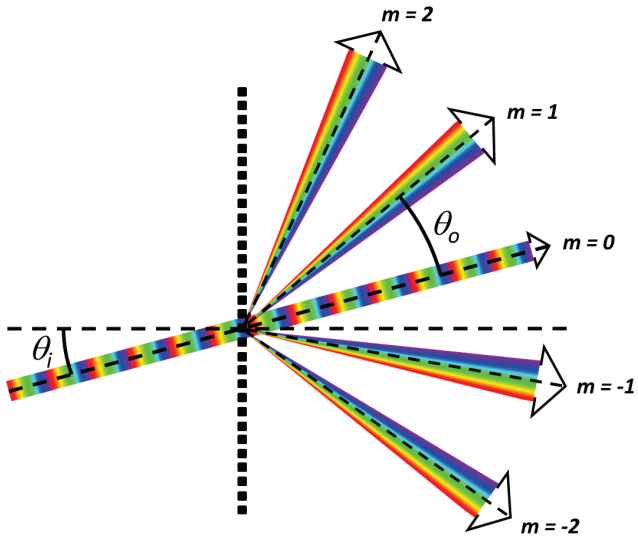

Figure 2.1. Schematic drawing of an amplitude transmission grating.

where a stands for the grating period. Two important properties of the diffraction gratings follow from Eq. (2.1). First, the grating period should be larger than λ at normal incidence and larger than $\lambda/2$ at grating incidence, otherwise there will be no diffraction. Second, the diffraction angle θ_m depends on the wavelength. This property gives diffraction gratings the ability to split light into its spectral components. This feature makes diffraction gratings very common optical element in spectrometers.

There exists a variety of diffraction gratings with different operational principles [1]. For example, the diffraction can originate from periodic modulation of the light amplitude, phase or both. In phase gratings, only the phase is modulated - e.g., by introducing a periodic difference in the optical path lengths across the beam, which results in periodic deformation of the transmitted wave front. These gratings are usually made of glass [19, 20] with etched periodic trenches. The difference in the refractive index in the grooves and in the glass stripes provides the necessary periodic variation in the optical path length. Phase gratings are superior compared to amplitude gratings because they insert less optical losses. Reflective diffractive gratings are usually also phase gratings. The optical path modulation in them is achieved by a periodic relief pattern of the reflecting surface of the grating [1]. In both reflective and transmissive gratings, the trenches can have different geometries: square in binary gratings, triangular in blazed gratings [1] and sinusoidal in sinusoidal gratings.

One of the important properties of diffraction gratings is the diffraction efficiency, which measures the amount of optical power diffracted into a designated direction. Phase gratings usually have the highest diffraction efficiencies because of low losses. If the optical path difference within the grating period is equivalent to a phase shift of π radians, the zeroth diffraction order disappears and all optical power turns out to be diffracted into higher diffraction orders. Sinusoidal gratings can have diffraction efficiencies as high as 100 % for the first two orders with $m = 1$ and $m = -1$ [21]. A reflective grating can be made to transfer the whole power exclusively into one of these orders. Most of the gratings mentioned above can be fabricated by using techniques introduced in this thesis.

2.2 Photonic crystals

A periodic stack of dielectric materials with different refractive indices is the simplest example of one-dimensional photonic crystal [2, 3, 4, 5, 6]. It is frequently used as a so-called Brag reflector [22, 23, 24], which reflects light within a certain prescribed frequency band. Such a structure is shown schematically in Fig. 2.2a. A wave, propagating through the stack experiences partial reflection at each interface. If the period of the stack is close to $\lambda/2$ (ideally, the optical thickness of each homogeneous slab must be $\lambda/4$), then every successive reflection from neighboring periods will be in phase with each other and, therefore, will interfere constructively. Thus, the incident light will totally be reflected back. The wavelengths at which the total reflection occurs form a so-called photonic band gap [25, 26, 27]. At these wavelengths light cannot propagate through the crystal normally to the slab interfaces. The photonic bang-gap width of a Bragg reflector made of $\lambda/4$ slabs is calculated as [28]

$$\Delta\lambda_B = \frac{4\lambda_B}{\pi} sin^{-1}\left|\frac{n_2 - n_1}{n_2 + n_1}\right|. \tag{2.2}$$

Bragg reflectors, which are also called dielectric mirrors, have a large area of applications because they do not cause optical losses and can be designed to reflect light in a specific spectral interval [22]. Such reflectors are used in laser cavities as frequency-selective mirrors. Optical fibers often incorporate distributed Bragg mirrors, e.g., to realize wavelength division multiplexing [29]. A stack of dielectric films can also de designed to minimize optical reflection and maximize the transmission, acting thus as anti-reflection (AR) coatings.

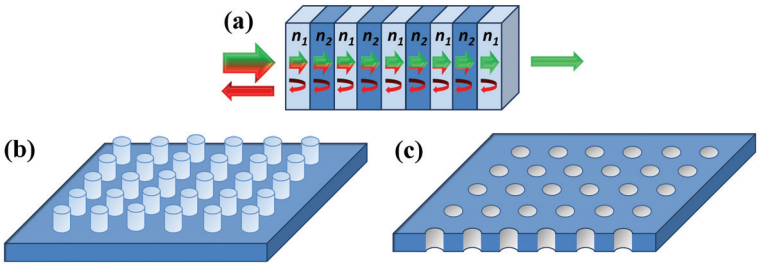

Figure 2.2. Schematic drawings of (a) a 1D photonic crystal (Bragg reflector) and 2D photonic crystals consisting of (b) dielectric pillars and (c) a dielectric slab with holes.

One-dimensional (1D) and two-dimensional (2D) periodic media cannot exhibit a total photonic band gap that is independent of the direction of light propagation. This can be achieved only in 3D photonic crystals [2, 30]. Examples of 2D photonic crystals composed of dielectric pillars and holes in a dielectric slab are, respectively, shown in Figs. 2.2b and 2.2c. Such structures can be used as waveguides with very interesting optical properties [30, 31, 32, 33]. For example, one can achieve a so-called self-collimation effect in these structures [34, 35, 36, 37]. It is based on the fact that, if the isofrequency contours (coined also as spatial dispersion curves) of the propagating Bloch modes have flat segments, optical beams with modal wave vectors within these segments will propagate in the slab without change of their transverse intensity profiles. This allows using such crystals for position and incidence-angle independent diffraction-free guiding of optical beams. By removing a thin stripe of the pattern, a narrow waveguide within such a 2D photonic crystal is created for light of a frequency within the crystal's band gap. Two-dimensional photonic crystals similar to those in Figs. 2.2b and 2.2c can be fabricated using the optical interference lithography described in this thesis. Three-dimensional crystals are more difficult to fabricate and, because of this, they are not as frequently used as 2D crystals. However, they can exhibit even more unusual optical characteristics, such as effective negative refraction [38, 39, 40, 41].

The band structure of the photonic crystal generally varies with the direction of the light propagation because of different pattern periods in different directions. 2D crystals have functionalities similar to 3D crystals except for being limited to one plane. A dielectric slab with voids or an array of pillars allow for position- and incidence angle-independent diffraction-free guiding of optical beams. A waveguide within the photonic

crystal can be created by removing a thin stripe of the pattern as mentioned above [30, 31, 32, 33]. Photonic crystals are capable of exhibiting super dispersion [42] and other unusual light-guiding properties.

2.3 Subwavelength gratings

Gratings with a period smaller than half the wavelength, also called subwavelength gratings, are not capable of causing diffraction according to Eq. (2.1). However, they can be used to control the light intensity and polarization. This section introduces operational principles and applications of such subwavelength gratings.

2.3.1 Wire-grid polarizers

Wire-grid polarizers are subwavelength gratings made in the form of an array of parallel metal nanowires on an optically transparent substrate [43, 44, 7]. Such a polarizer transmits light with the electric-field vector directed perpendicularly to the wires. The operational principle of the device is as follows. For an optical wave incident onto a wire-grid polarizer, the electric field can be resolved into two orthogonal components, one perpendicular to the wires (y-component in Fig. 2.3) and the other parallel to them (z-component). The z-component of the field drives conduction electrons in the metal along the wires. The extended length of each wire makes the electron movement unrestricted in the z-direction, resulting in an optical response of the grid being equivalent to that of a thin metal film. The transmission of incident z-polarized wave is nearly perfectly cancelled by the destructive interference with the field radiated by the wires in the forward direction. Analogously, since significantly elongated noble-metal nanoscatterers exhibit strong resonance for longitudinal excitation at long, infrared, wavelengths, the scatterers will radiate out of phase when driven with shorter, visible wavelength. Thus, z-polarized visible light is mostly reflected by the device.

The y-component of the incident wave will excite much weaker currents in the nanowires because the electrons' movement is now restricted to the wire width. In addition, the field, radiated by the wires in the forward direction will be nearly in phase with the transmitted incident field that is now *red-detuned* from the transverse short-wavelength resonance. Thus, the majority of y-polarized light will be transmitted by the polarizer, and

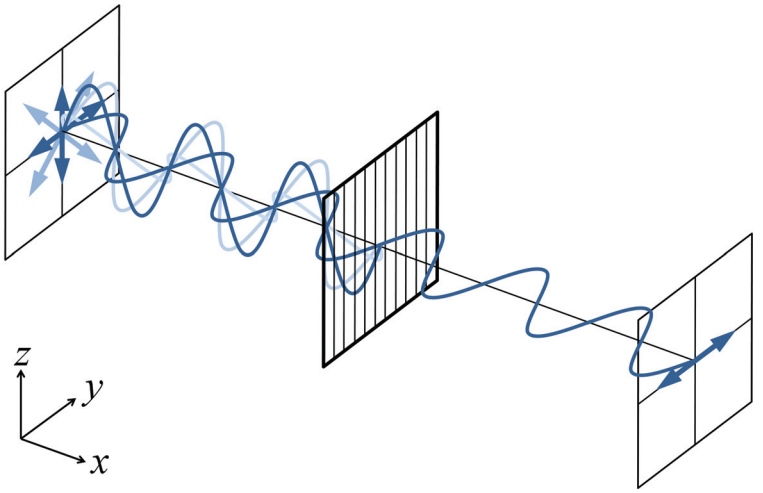

Figure 2.3. Transmission of light through a wire-grid polarizer.

only a small fraction of it will be reflected. However an alternative design of the wire-grid polarizer with inverse operation principles was proposed recently [45].

The nanowires are made of metal and, therefore, some absorption of light is inevitable [46]. An additional loss can take place due to scattering at metal imperfections. These losses are the main disadvantage of wire-grid polarizers. They will, though, have several important advantages over other beam-splitting and absorptive polarizers. One of them is the extremely wide operation wavelength band, allowing for coverage of the whole visible range. The angle of incidence can be essentially arbitrary if the wire period is smaller than half of the shortest working wavelength. Wire-grid polarizers can be very thin, which makes them irreplaceable in compact, integrated optical devices. They are relatively inexpensive and, compared to plastic polarizers, are durable against aging, chemically aggressive environments and high temperatures [47]. In particular, because of this latter reason, they can be used at high optical intensities. The extinction ratio of these polarizers is on average about 1000, which is a reasonably high value. These properties make wire-grid polarizers very attractive, especially in the liquid-crystal display technology. High quality wire-grid polarizers can be manufactured by using the nanofabrication techniques presented in this thesis.

2.3.2 Wave plates

Not only transmissive, but also reflective subwavelength gratings can alter the polarization state of light. In this case, however, it is possible to convert the state to any elliptical polarization of interest. The device can thus act as a wave plate [8, 48]. Metal nanogrid wave plates belong to this class of optical devices. They operate as follows. Light incident at such a wave plate, can as in the previous example, be split into two orthogonal polarization components, into TM (with the electric field directed along the grooves) and into the orthogonal TE component (see Fig. 2.4). The TM-polarized component is mostly reflected from the top facets of the ridges while the TE-polarized light penetrates inside the grooves and is reflected from the bottom of the trenches. Thus, the reflected TE component has a longer optical path compared to the TM component. This results in accumulation of an additional phase by the TE component and this phase is proportional to the groove depth. The reflected TE and TM components interfere, producing a beam with a new polarization state. By varying the pattern depth any pase difference between the TE and TM components can be obtained. Furthermore, a single device can at different wavelengths operate as a quarter- and a half-wave plate. Similarly to wire-grid polarizers, metal nano-grid wave plates have a broader working frequency band than conventional transmissive wave plates. However, deep grooves in a metal sample are very difficult to manufacture. In addition, inevitable small imperfections can cause noticeable scattering and resonant absorption of light. In spite of this, we have succeeded to fabricate such a reflecting wave plate that shows reasonably good optical characteristics (see Publication III). Previously, only transmissive wave plates in the form of a subwavelength grating have been demonstrated to have a high optical quality [47].

2.3.3 Nanostructured antireflection coatings

Antireflection (AR) coatings are used to minimize the fraction of light reflected at the interface between two media [10]. A conceptually simple form of an AR coating is a graded-index film, matching the refractive indexes of, say, air and the substrate at the corresponding boundaries (see Fig. 2.5a). Light incident on the substrate would pass the film adiabatically without any reflection [49]. Being simple in the operational principle, such films are very difficult to manufacture, e.g., due to lack of solids

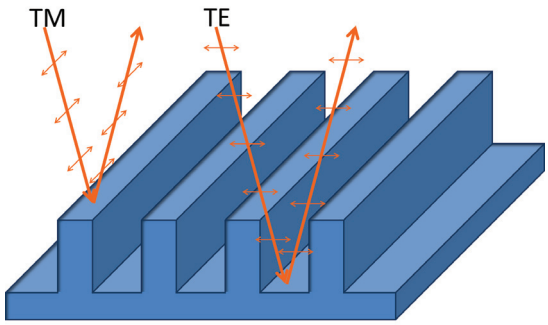

Figure 2.4. Schematic drawing of a metal nanogrid wave plate.

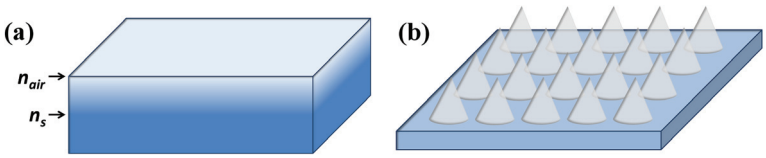

Figure 2.5. Schematic drawings of (a) a graded-index medium, (b) moth-eye antireflection coating.

with a refractive index close to 1. Conventionally, antireflection coatings are made with a stack of layers of low and high values of their refractive indices [50, 51, 52]. Such AR coatings, however, are rather thick. In addition they are rather sensitive to both the wavelength and the angle of incidence of the light.

A gradually changing effective refractive index can be obtained in nanostructured coatings. The so called moth-eye AR coating [53, 54, 55, 56, 57] shown in Fig. 2.5b is one of them. This coating consists of transparent cones. The cones are arranged in a periodic array with a period that is smaller than the wavelength. When illuminated from above or below, the cone structure acts as a homogenious material with an index of refraction gradually changing between 1 and the index of the substrate. Moth-eye antireflection coatings with a thickness of a small fraction of the wavelength are able to suppress reflection down to 0.1 % in the entire visible spectral range [58]. Furthermore, the coatings operate well also at tilted incidence. These properties make nanostructured coatings of this type very attractive in view of liquid-crystal and other display applications as well as in solar cells. As a disadvantage, one could mention that small surface imperfections of the coating can lead to a significant light scattering. Furthermore, the nanocones are not necessarily very stable mechanically.

2.4 Plasmonic nanostructures

Most metals are highly reflective to visible light [59, 60, 61]. However, under special conditions light can be very efficiently absorbed via resonant excitation of collective oscillations of conduction electrons at the metal surface. These excitations are called surface plasmons [62, 63, 64, 65, 66], which are localized solutions of the wave equations at a metal-dielectric interface. The localization means that the electromagnetic field created by the excited electrons exponentially decays along the normal to the interface in both directions. The wave vector and the Poynting vector of the field are parallel to the interface if the interface is flat. Figure 2.6a shows a metal-dielectric interface lying in the xy-plane and an optical wave incident upon it. The wave is TM-polarized. A TE-polarized wave is not able to excite surface plasmons. The parameters $\varepsilon_m(\omega)$ and $\varepsilon_d(\omega)$ are the complex frequency-dependent dielectric functions of the metal and the dielectric, respectively. Solving for the wave equation

$$\nabla \times \nabla \times \vec{E}(r,\omega) - \frac{\omega^2}{c^2}\varepsilon(r,\omega)\vec{E}(r,\omega) = 0, \tag{2.3}$$

we can obtain the dispersion relations for the propagation direction along the interface (the corresponding wave number is k_{sp}) and perpendicular to it ($k_{m,z}$ and $k_{d,z}$) in the metal and the dielectric, respectively. These relations are

$$k_{sp} = (\omega/c)\sqrt{\frac{\varepsilon_m\varepsilon_d}{\varepsilon_m+\varepsilon_d}}, \tag{2.4a}$$

$$k_{m,z} = (\omega/c)\sqrt{\frac{\varepsilon_m^2\varepsilon_d}{\varepsilon_m+\varepsilon_d}}, \tag{2.4b}$$

$$k_{d,z} = (\omega/c)\sqrt{\frac{\varepsilon_d^2\varepsilon_d}{\varepsilon_m+\varepsilon_d}}. \tag{2.4c}$$

For the solution to be bound to the surface, $k_{m,z}$ and $k_{d,z}$ are required to be purely imaginary. This leads to the following condition

$$\begin{cases} \varepsilon_m(\omega) + \varepsilon_d(\omega) < 0 \\ \varepsilon_m(\omega)\varepsilon_d(\omega) < 0. \end{cases} \tag{2.5}$$

This condition implies that, if $\{Im(\varepsilon_m(\omega))\}$ is small, $\{Re(\varepsilon_m(\omega))\}$ must be negative and have an absolute value larger than $\varepsilon_d(\omega)$. This condition can easily be satisfied by using noble metals. However, surface plasmons cannot be excited by direct illumination of the metal surface because the wave vector in free space is too short compared with that of the surface plasmon-polariton of the same frequency ω. Usually surface plasmons are

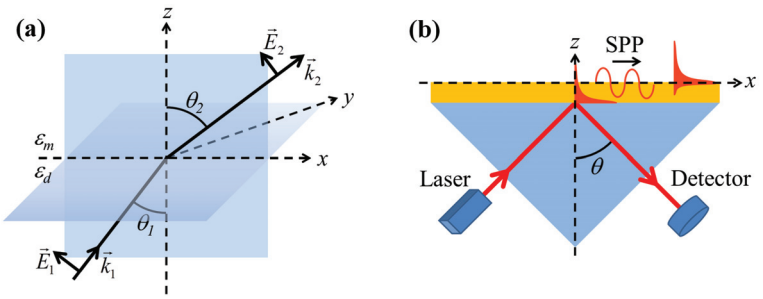

Figure 2.6. (a) A schematic representation of a light wave passing through a metal-dielectric interface. (b) Excitation of surface plasmon polaritons in the Kretschmann configuration.

excited by means of optical evanescent waves at glass-air interface under the condition of total internal reflection (TIR) [67, 68, 69, 70]. As an example, Fig. 2.6b shows a setup, called Kretschmann configuration, in which a thin metal film on a prism surface is illuminated in TIR geometry. At an angle θ_{sp}, at which the wave vector of the plasmon is equal to the tangential component of the wave vector of the incident light, $k_x = k_0 n_d sin\theta_{sp}$, a surface plasmon-polariton will be excited. Here n_d stands for the dielectric refractive index of the prism.

On the other hand, in subwavelength-sized metal nanoparticles, the plasmon oscillations are localized to a strongly curved surface of the particle, and the conditions for their excitation substantially differ [71, 72, 64, 73, 74, 75]. In fact, plasmons can now be excited by direct illumination even in vacuum.

For a small metal sphere, one can apply a quasistatic approximation and, neglecting all multipole excitations higher than the dipole one, derive the following expression for the particles dipole polarizability

$$\alpha(\omega) = 4\pi\epsilon_0 R^3 \frac{\varepsilon_m(\omega) - \varepsilon_d}{\varepsilon_m(\omega) + 2\varepsilon_d}. \tag{2.6}$$

Here R is the radius of the nanoparticle. The excited dipole moment is then given by $\vec{p} = \alpha(\omega)\vec{E_0}$ where $\vec{E_0}$ is the incident field. Suppose that $\vec{E_0}$ is directed along z and the particle is centred at (x, y, z) = (0,0,0). The maximum of the field amplitude at the surface can be calculated as

$$\vec{E}(0, 0, R) = \frac{2\vec{p}}{4\pi\varepsilon_0\varepsilon_d R^3} \equiv \sqrt{f}\vec{E}_0, \tag{2.7}$$

where f is the intensity enhancement factor given by

$$f = \frac{\alpha^2(\omega)}{4\pi^2\varepsilon_0^2\varepsilon_d^2 R^6}. \tag{2.8}$$

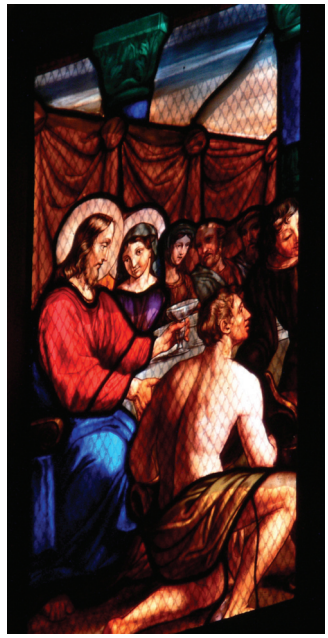

Figure 2.7. Picture of a stained glass window from Milan Cathedral [picture taken by the author of this thesis]. The coloring is achieved by incorporation of metal nanoparticles into the glass.

This factor is seen to be inversely proportional to R^6. As an example for a gold nanoparticle with R= 5 nm, located in water, the enhancement factor is $f \approx 3000$.

The scattering cross-section of a nanoparticle is

$$\sigma_{scatt} = \frac{k^4}{6\pi\varepsilon_0^2}|\alpha(\omega)|^2, \tag{2.9}$$

where k is the wave number in the surrounding medium. The extinction cross-section, σ_{ext}, which is the sum of the absorption and scattering cross-sections is given by

$$\sigma_{ext} = \frac{k}{\varepsilon_0}\mathrm{Im}\left[\alpha(\omega)\right]. \tag{2.10}$$

Substitution of Eq. (2.6) into Eqs. (2.9) and (2.10) leads to the important conclusion that σ_{scatt} depends on R^6 while σ_{abs} only on R^3. This means that light extinction by large nanoparticles is mostly through scattering while for small particles it is dominated by absorption. The transition between the prevailing regimes is associated with a distinct change in the transmission and reflection spectra. Figure 2.7 shows a fragment of a stained glass window in the Milan Cathedral. The various colours are due to specific plasmonic bands of metal nanoparticles incorporated in the glass.

For non-spherical particles, the resonance condition splits into several ones to describe the resonant excitations along the different directions. Often such particles can be modelled as spheroids. By applying the quasi-static approximation, one can derive the following expression for the particle polarizability,

$$\alpha(\omega) = V\epsilon_0 \frac{\epsilon_m - \epsilon_d}{L_i\epsilon_m(\omega) + (1 - L_i)\epsilon_d}. \tag{2.11}$$

Here V stands for the volume of the particle and L_i are geometrical factors describing the longitudinal and transverse plasmonic resonances. These factors depend on the spheroid aspect ratio of the spheroid. The longitudinal and transversal resonances are always red and blue shifted, respectively, from the resonant frequency of a spherical particle. It should be noted that the quasi-static approximation is not valid for long, rod-like metal nanoparticles. These particles can be treated as finite pieces of a nanowire supporting propagating plasmon waves.

The plasmon resonances, which usually lie in the visible and infrared spectral regions, depend on the particle material, size, shape as well as on the way the nanoparticles are distributed on the surface and in the volume of the substrate [72, 64]. This multitude of parameters provides flexibility for the design of various plasmonic devices, where the final result depends not only on design requirements but also on fabrication capabilities. Arranging nanoparticles in periodic arrays further boosts local plasmon resonances leading to local field enhancement by several orders of magnitude [76, 77, 78]. One of the applications of the metal nanoparticles is to fabricate substrates for surface enhanced Raman spectroscopy (SERS). Raman scattering is an inelastic scattering process via energy exchange between a photon and the vibrational states of the molecule [79, 80, 81, 82, 83, 84]. The scattering process is schematically described in Fig. 2.8. While in the classic Rayleigh scattering process the molecule returns from an excited virtual state back to the original state, in the Raman process it returns to an excited vibrational state. The scattered Raman photon is then at frequency $\nu_r = \nu - \nu_{vib}$, where $h\nu_{vib}$, corresponds to the energy of the excited vibrational mode in the molecule. There is also the possibility that the molecule is initially in an excited vibrational state and the scattering takes place to the non-excited ground state. The former Raman process is called Stokes scattering and the latter anti-Stokes scattering.

The Raman spectrum is unique to the molecules under study and can therefore be used for non-destructive chemical analysis [85, 86]. However,

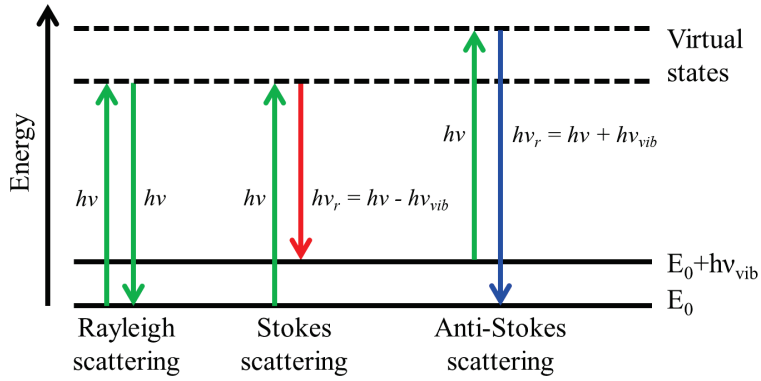

Figure 2.8. Raman scattering energy diagram.

Raman scattering cross-sections are on average 14 orders of magnitude smaller than typical fluorescence cross-sections [83, 84]. This tremendous difference in strength implies use of sophisticated ultra-sensitive equipment or development of special techniques to enhance the Raman scattering effect.

The Raman scattering cross-section can be enhanced by adsorbing the analyte molecules onto a surface which exhibits strong local near-field amplification of the light's electric field via surface plasmon excitations. This technique, called *surface enhanced Raman spectroscopy*, is able to enhance the Raman signal by up to $10^8 - 10^{14}$ fold [83, 84] compared to a bulk analyte. Thus, it is possible to detect even a single molecule by Raman detection [83, 84]. Suitable surfaces can be obtained by placing metal nanoparticles on dielectric or semiconductor substrates.

The surface enhancement is a two-stage process. First, an incident laser beam excites surface plasmons at the nanoparticles, giving rise to a strong local near-field intensity amplification f according to Eq. (2.11). This enhanced near field stimulates a proportionally stronger Raman scattering phenomenon at the adsorbed molecule. Then the generated Raman signal further excites surface plasmons at the metal nanoparticle resulting in an additional near-field enhancement with a strength similar to the original f. Thus, the total intensity enhancement of the Raman scattering *becomes* $f_R \approx f^2$. Following the example of a golden nanoparticle from above, the amplitude enhancement of the Raman signal will be $f_R \approx 10^7$.

Surface enhanced Raman spectroscopy can be used for quick and inexpensive chemical analysis in medicine, chemistry and environmental sciences. However, the main challenge is still the lack of simple and reliable fabrication techniques for nanopatterned SERS substrates. The

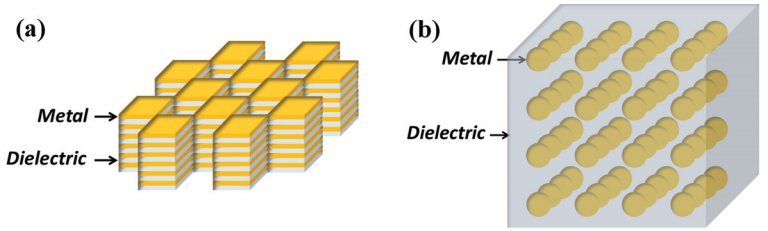

Figure 2.9. Various metamaterial designs.

nanofabrication process, presented in this thesis, can be used to manufacture high-performance SERS substrates.

The strong dependence of the surface plasmon resonances on the surroundings can be used to build highly sensitive plasmonic sensors. There exist many variations of these sensors, including a thin metal film on top of a prism in the Kretschmann configuration, periodic micro- and nanopatterns of gold or silver on a substrate, and individual metal particles. Adsorbing even just a molecular monolayer of an analyte onto the surface of such a sensor can cause a significant shift of the plasmon resonance frequency. This shift is observed either in a direct spectroscopic measurement or via a change in the sample reflectivity. A plasmonic sensor in the form of a periodic array of metal nanostructures can be manufactured using the nanofabrication techniques presented in this work. An example of such a sensor is discussed in Publication II.

Recent progress in nanofabrication techniques has opened us an exciting possibility to create “artificial atoms”, in the form of nanoparticles, and “metamaterials” made of them. The nanoparticles can be designed to provide the material with extraordinary optical properties that cannot be found in nature. For example, optical metamaterials can exhibit optical magnetism and negative refraction as well as produce extraordinary phenomena such as perfect focusing and optical cloaking. For the material to be seen by light as homogeneous, its lattice constant must be smaller than the light wavelength. To exhibit negative refraction, the material must have negative permittivity and negative permeability. This can be achieved by using three-dimensional arrays of metal nanostructures, because metals naturally have negative permittivity at visible light frequencies and the structures can be designed to provide negative permeability under special plasmonic resonance conditions. Three-dimensional metamaterials are difficult to fabricate if the structures have a sophisticated geometry. Some relatively simple configurations for obtaining negative-

index materials, such as a double-fishnet structure consisting of a perforated stack of metal and dielectric layers have been proposed and already demonstrated in practice [38, 39, 40, 41]. Examples of these and other metamaterial designs are shown in Fig. 2.9. Similar metamaterials can be fabricated using the techniques presented in this thesis.

3. Photolithographic methods of nanofabrication

3.1 Principles of photolithography

Photolithography is a technique to transfer light patterns first onto a layer of photosensitive material, to create a mask, and then, through the mask, to another material that can be in the form of a thin film or simply be the bulk of the substrate [87, 88, 89]. General steps of the lithographic process are shown in Fig. 3.1. In the first step a photosensitive polymer called photoresist is deposited on the surface of a flat substrate that can be preliminarily coated with another material [see Fig. 3.1(I)] [87, 90]. Then the photoresist is selectively exposed to light [Fig. 3.1(II)], which changes the chemical composition of the polymer [90, 91, 92, 93]. The next step is the development of the photoresist [Fig. 3.1(III)] and removal of the exposed parts of the material [94]. This step yields the photoresist mask that is subsequently used to pattern the material of interest, usually by wet or dry etching [Fig. 3.1(IV)]e [87, 88, 89]. The final stage [Fig. 3.1(V)] is stripping the mask from the sample [94]. Alternatively, the patterned photoresist can be covered with a layer of another material, e.g. gold (see Fig. 3.1(VI)) [87, 88]. Removing the photoresist will then result in a pattern of this material repeating the photoresist openings [Fig. 3.1(VII)]. These two steps comprise the so-called lift-off technique [87, 88].

The lithography process usually involves a large number of auxiliary methods and specific steps that fulfil each particular requirement. Quite often the surface of the substrate wafer is modified prior to deposition of the photoresist. This modification can be done by means of various techniques, such as sputtering [95, 96] and evaporation [97, 87, 88], atomic layer deposition [98, 99, 100], electroplating [87, 88], chemical vapor deposition [101, 102], oxidation [87, 88] and a number of epitaxial deposition

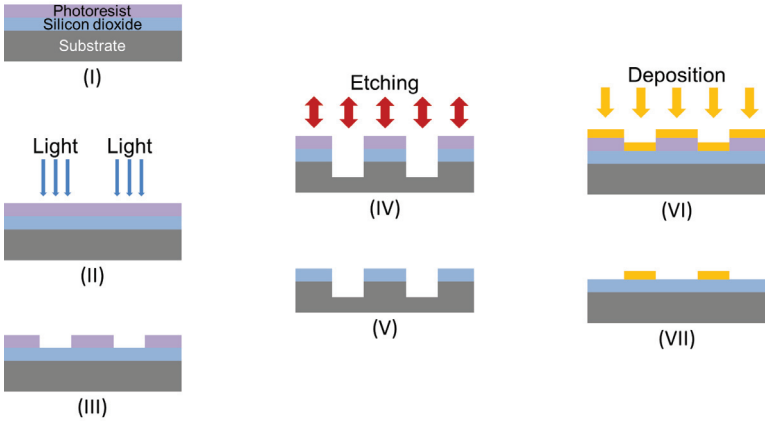

Figure 3.1. Basic steps of photolithography: (I) Coating the substrate with a layer of photoresist and, if necessary, with an additional intermediate material; (II) exposure to a light pattern; (III) development and removal of the exposed (or unexposed) photoresist; (IV) etching through the obtained photoresist mask; and (V) stripping the mask. Alternatively, one can use the photoresist pattern in a lift-off precess, shown in steps (VI) and (VII) for an example of obtaining a pattern of gold.

techniques [87, 88]. Alternatively, the surface of the wafer can be modified by ion implantation [87, 88]. Then, as a rule, a monolayer of a special adhesion promoter is deposited onto the wafer to improve bonding of the photoresist to the substrate. After this, the photoresist is spin-coated onto the wafer from a solution [90]. To dry the photoresist, the wafer is subjected to a soft-bake process [90], in which the solvent is evaporated as a result of heating of the sample.

The photoresist film can be exposed selectively ither through the photomask or by using a maskless exposure technique [87, 88, 89, 103, 104, 105, 106]. Conventional photomasks are usually made of a transparent plate with an opaque pattern of, e.g., chromium on its surface. If the wafer already contains some pattern, the photomask should be aligned relative to that pattern. Exposure of the photoresist requires several additional considerations. If the surface of the substrate is highly reflective and the pattern contains relatively small features, a special antireflective coating must be introduced beneath the photoresist to eliminate the formation of unwanted optical standing waves [104, 105, 106, 107, 108, 103]. These standing waves can significantly roughen the photoresist mask pattern. The exposure time should be carefully selected to achieve correct feature sizes and vertical walls of the mask. Since conventional photoresists are sensitive to temperature and humidity variations as well as to stray light, the exposure should be done in a specially equipped clean room. If the pat-

tern elements of the mask are small, scattering and diffraction at the pattern edges should be controlled. The scattered light passing through the mask can be suppressed by using phase-shift correction elements. Such elements introduce an additional contribution to the transmitted light shifted in phase by π radians. This light interferes destructively with the unwanted scattered light, drastically improving the pattern quality. Photomasks allow for exposing an entire wafer in a few seconds, which makes their use perfect for mass production. However, any change in the designed exposure pattern requires a new photomask, whose fabrication is an expensive and time consuming process.

The photoresist can also be selectively exposed by guiding a beam of light or electrons on its surface [87, 109, 110, 111]. Such exposure methods are not based on the use of a photomask and are therefore called maskless. They have several advantages over conventional photolithography, such as the ability to change pattern even during the exposure. Electron beam lithography can have very high resolution, on the order of 1 nm. However, since the system can expose at once only an area equal to the beam cross section, drawing a pattern on the entire wafer is time consuming and consequently extremely expensive. Therefore, such direct writing techniques are used mostly for prototyping and to fabricating photomasks, but never for mass production.

The exposed photoresist differs in its chemical composition from the unexposed one. To form a mask for further etching of the substrate, the photoresist must be developed [94]. In this process only exposed or unexposed photoresist is removed from the sample using a chemical solution (developer). Two basic types of photoresist exist: If the photoresist is positive, the exposed portion of it is dissolved in the developer [87, 94]. On the other hand, the exposed parts of a negative photoresist are insoluble in the developer [94]. The polymer material and developer are different for positive and negative photoresists, and it is usually impossible to apply both positive and negative patterns to the same photoresist film. However, a few special image-reversal photoresists, which allow for switching between the positive and negative patterns, have been developed [94].

An important parameter of each photoresist is its resolution. It depends on the chemical composition of the polymer. Usually the resolution obtained with a negative photoresist is lower than that with positive ones because long polymer chains are formed during the exposure. The development step always ends with rinsing the sample in, e.g., water in order

to remove the developer and all unnecessary products of the associated chemical reactions.

Photoresist masks can be used in many different ways to selectively modify a thin film or the substrate surface. Two fundamental types of etching are wet etching and dry etching [87, 88, 112, 113]. In wet etching, the wafer is submerged in an etchant solution that chemically reacts with the surface, unprotected by the photoresist mask. The reaction products should be soluble or volatile. As a result, the material is selectively removed from the unprotected areas. In dry etching, the substrate is attacked by active gases, usually oxygen, fluorine or chlorine, which remove the material from the wafer areas unprotected by the photoresist. In order for dry etching to work, the reaction products have to be in gaseous form. The most important parameters in any etching are the etching profile and selectivity, also called the etching ratio. The etch profile is determined by the way the etching front advances into the wafer. Isotropic etching is characterized by hemispherical propagation of the etching front. In anisotropic dry etching, the etching fronts propagate faster in some particular directions, but in anisotropic wet etching, the front propagates as a plane wave along the crystal axes. Isotropic etching of silicon through a rectangular opening in the mask would yield a cavity with a hemispherical profile. Dry etching, in contrast, could give a rectangular cavity. However, anisotropic etching in potassium hydroxide solution that etches the material in the $< 100 >$ direction 200 times faster than in the $< 111 >$ direction will yield a triangular shape for the etch cavity [87].

In anisotropic dry etching, the wafer is inserted into low pressure plasma discharge in the etchant gas. The discharge makes the ions fly in one direction and the wafer is usually inserted perpendicular to this direction. The process is called reactive ion etching (RIE) [114, 115, 116]. RIE is accompanied by sputtering of the etched material due to bombardment by energetic ions. An additional control of the etching profile can be obtained by using an additional gas that continuously forms a thin passivation film on the wafer. This film can completely suppress the lateral etching while only insignificantly slowing the etching process in the desired direction.

The selectivity mentioned above concerns the ratio of the etching speed of the targeted material to the etching speed of the photoresist mask. A larger value of this parameter allows etching of the same amount of the material through a thinner mask. Thinner masks are easier to fabricate and they cause less distortions during deep etching. The etch ratio can

be rather small, e.g., 2-3, when etching sapphire via a chromium mask in an inductively coupled plasma RIE (ICP-RIE) [117]. It also can be very large, such as 10^6 when etching silicon through alumina in similar ICP-RIE [118, 119, 120, 121]. When the etching is completed, the mask is stripped usually with the help of a solvent or with oxygen plasma.

For some materials, such as gold, dry etching is impossible due to the lack of gases forming volatile chemical products with the material. In such cases patterning can be accomplished by using ion milling – a pure sputtering process. Ion milling is a universal method, applicable to almost all materials, but it is simultaneously very aggressive to the mask.

A completely different way to pattern metals and other materials is to use a liftoff technique [87, 88]. In this technique a wafer with a polymer mask is first covered with metal or another material. Then the sample is submerged into a solvent that dissolves the polymer. The process lifts off the material that was on top of the mask, bul leaves the material deposited on the open areas of the wafer. The liftoff process is, however, difficult to use in mass production because it is slow and requires the mask to have clean walls and the deposited metal layer to be much thinner than the mask.

If the patterns to be created are periodic, it is customary to use optical interference lithography (IL) [103, 104, 105, 106, 122]. This maskless technique relies on using interference patterns created by two or more intersecting coherent laser beams to expose a photoresist. Two beams intersecting at an angle of 2θ will create a periodic interference fringe pattern with a period of a $= \lambda/(2sin\theta)$ and a sinusoidal intensity profile [122]. Interference lithography is a simple and inexpensive technique that has several advantages over the other mentioned techniques. It does not require a photomask nor sophisticated optics. Still an entire wafer can be exposed at once. The pattern period can be easily adjusted in a wide range from tens of micrometers down to half a wavelength of the exposure light by changing the angle θ. The technique provides a perfect long range periodicity. Quite complex mask patterns can be produced by overlapping several interference patterns or by applying several subsequent exposures with different orientations of the sample [122]. However, the use of coherent light can lead to formation of multiple standing wave patterns in the photoresist film due to non-negligible reflections at the interface between different materials [108, 103]. These unwanted interferences can be reduced by making the photoresist film sufficiently thin or

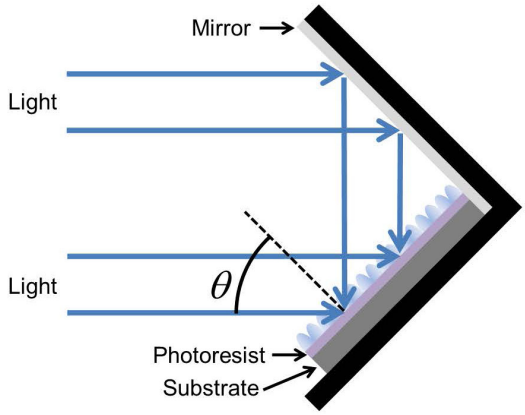

Figure 3.2. Lloyd interferometer setup.

by using a highly absorbing or antireflecting coating [87, 104, 106]. Since the exposure light has a sinusoidal intensity profile, vertical walls in the mask can only be achieved by using a *binary* photoresist. This photoresist changes its state abruptly after exposure to a specific dose of radiation. Binary photoresists are beneficial also because they give an opportunity to control the pattern sizes by adjusting the exposure time.

One of the most stable and reliable optical setups used to create interference fringe patterns is shown in Fig. 3.2. The system is called Lloyd interferometer. In this setup an incident beam is split in two parts. The top part is incident onto a mirror and then reflected to the photoresist film. The bottom part of the beam, being directly incident onto the photoresist film, interferes with the reflected part, forming an interference pattern at the surface of the photoresist film. The angle between the mirror and the sample plane is fixed to 90°. Rotating the whole setup with respect to the incident beam, one can adjust the interference pattern period in a wide range, from tens of microns to half the wavelength according to the expression $a = \lambda/(2sin\theta)$. The Lloyd setup has a rigid construction, which makes it robust to vibrations and air turbulence. Vibrations of the whole interferometer affect both beam parts in the same way and, hence, cause no distortion to the interference pattern.

3.2 Azopolymer-based lithography

Azobenzene-containing polymers are alternative photosensitive materials that can be used in photolithography [123, 124, 125, 126, 127, 128, 129, 130]. These polymers, when illuminated with an optical interfer-

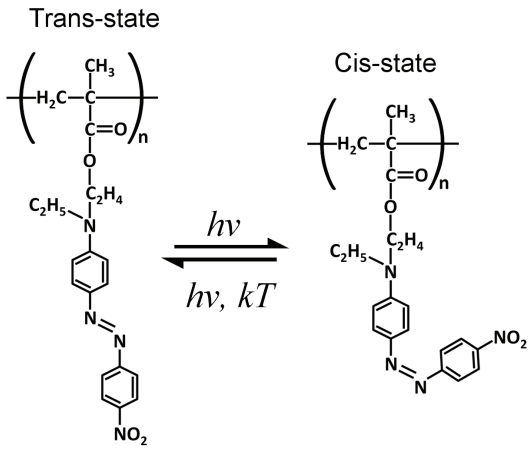

Figure 3.3. Trans-cis isomerisation of azo-polymer poly(disperse red 1 acrylate).

ence pattern, can physically migrate, e.g., from illuminated to dark areas [131, 132]. The process yields a replica of the incident irradiation pattern in the form of a surface relief grating (SRG) [133, 134, 135, 136, 137]. In contrast to photoresists, no chemical development is needed to obtain such relief patterns.

Azopolymer molecules consist of polymer chains bonded to azobenzene moieties. The azobenzene molecules have two isomer states - *trans*-state and *cis*-state (see Fig. 3.3) [131, 132]. Normally the molecules are in the straight *trans*-state. Then, by exposing them to light (usually blue), they can be rapidly switched to the bent *cis*-state. This molecular-level switching results in a decrease of the distance between the para-carbon atoms of the azobenzene from about 10 Å to 6 Å. From the *cis*-state the molecules thermally relax to the original *trans*-state. The relaxation transition can be accelerated by heating or by illuminating the sample with light at a different wavelength.

Under continuous spatially modulated illumination, azopolymer molecules undergo the *trans-cis-trans* photoisomerization cycles leading to a macroscopic mechanical motion of the polymer [130]. It is remarkable that in amorphous azopolymers this motion takes place at a temperature well below the glass transition temperature [131]. Moreover, the material migration is highly sensitive to the polarization of the incident light [131]. The azobenzene molecules in their trans form are more efficiently excited by light that has the electric field vector along the molecules. Thus an SRG inscription is far more efficient when accomplished with p-polarized or circularly polarized interfering beams than with s-polarized or unpolarized

light. This makes it possible to inscribe surface relief gratings under ordinary room lighting conditions and using interference patterns with flat intensity profiles but spatially varying polarization. In principle, the SRG modulation depth increases when the intensity contrast of the polarization component perpendicular to the interference fringes becomes higher. In addition, the insensitivity of the polymer to unpolarized light makes the inscribed patterns stable against stray light. Furthermore, azopolymers are not very sensitive to temperature and humidity variations, and the patterned samples have a very long shelf lifetime. Also, azopolymers tolerate well overexposure, owing to which multiple exposures are easy to perform. All these properties make azopolymer a favorable alternative to photoresist for applications in optical interference lithography.

Sinusoidal diffraction gratings for optical waves, e.g., transmissive phase gratings, can be fabricated by the direct inscription of an SRG into an azopolymer film. In this case practical maximum achievable SRG modulation depth is about twice as large as the thickness of the original azopolymer film. Then, coating the SRG with a reflective material, such as metal, can be used to obtain a reflective phase grating. Usually, diffraction gratings fabricated with the help of a photoresist are binary, while the SRGs recorded in an azopolymer film have a smooth sinusoidal profile. As a consequence, azopolymer gratings can have lower scattering losses. In fact, reflective sinusoidal gratings can yield even 100 % diffraction efficiency into the first order under special conditions [138, 21].

Quite recently SRGs were proposed as a tool to micro- and nanostructuring other materials, raging from polymers to metals and semiconductors [139, 140, 141]. The patterning techniques can be divided into three basic groups. In the first group, azopolymer surface relief patterns are used as molds [142, 143, 144, 145]. The technique is similar to nanoimprint lithography [146]. The second group makes use of the so-called directional photofluidization lithography (DPFL) that combines methods of microfluidics with optical control of azopolymer microstructures [139]. In the third group, SRGs are used as an etch mask similarly to conventional photoresist masks. The fabrication techniques described in this thesis deal with the third approach and, therefore, in the following, that technique will be described in more detail than the two other approaches.

The molding technique resembles nanoimprint lithography. It consists of the following steps: First, a clean substrate is spin-coated with an azopolymer film and an SRG is inscribed on its surface. Then, the pat-

terned substrate is coated again with a polymer, such as poly(methyl methacrylate) (PMMA) or polydimethylsiloxan (PDMS), from a solution that is solidified by drying or curing. The last step is to peel off the polymer that contains a reversed (imprinted) SRG pattern. The polymer sample obtained in this way can be used as it is, e.g., as a diffraction grating, or as a stamp for further replication of the original SRG. Also, if the imprint is made on a thin polymer film bonded to a solid substrate, then the film can be used as an etch mask to pattern the substrate.

In the directional photofluidization lithography, an azopolymer is first shaped by using a soft stamp made of, e.g., PDMS. This results in a two-dimensional pattern, usually in the form of periodic lines or islands. Then, the stamp is removed and the azopolymer array is reshaped by exposing it to polarized light that in addition can be spatially modulated. The photoinduced motion of the azopolymer molecules can result in so-called "self-perfection by liquefaction" that can significantly improve the shapes and the surface quality of the azopolymer structures [147].

It has been recently realized that, potentially, surface relief gratings can be used as etching masks for surface patterning of the substrate. In particular, we have proposed and experimentally demonstrated the use of SRGs as masks for dry etching of silicon, metals and other materials (Publications I and II). This method allows one to fabricate large-area periodic arrays of various nanostructures, and the technique has several advantages over the conventional photoresist-based lithography, as has already been mentioned. The basic steps of the azopolymer-based interference lithography are presented Fig. 3.4. In the first step, a clean silicon substrate is spin-coated with a 100 nm thick azopolymer film and an SRG is inscribed on its surface using an interference pattern of two p-polarized or circularly polarized laser beams. In our experiments we have used a Lloyd interferometer described in the previous section. A single exposure gives a one-dimensional SRG [see Fig. 3.5(a)], while several subsequent exposures applied to a rotated sample can yield more sophisticated two-dimensional patterns [Fig. 3.5(b)]. For the obtained SRG to be applicable as an etch mask, the polymer is in the next step removed from the pattern trenches by anisotropic RIE in oxygen. Owing to the sinusoidal cross section of the pattern, the width of the remaining polymer stripes can be adjusted during the RIE by the etching time. Next, the obtained mask [Fig. 3.6(a)] is used to dry-etch the substrate, after which the mask is removed by wet etching.

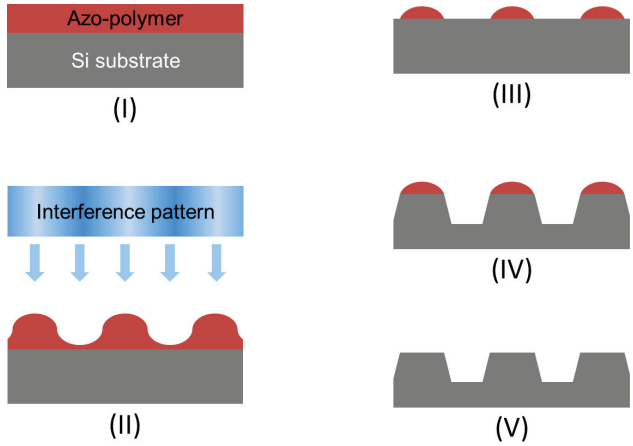

Figure 3.4. Schematic illustration of the fabrication process using a soft azopolymer mask: (I) spin-coating of an azopolymer thin film, (II) SRG inscription, (III) partial etching of the polymer in O_2, (IV) dry etching of Si, and (V) stripping the mask.

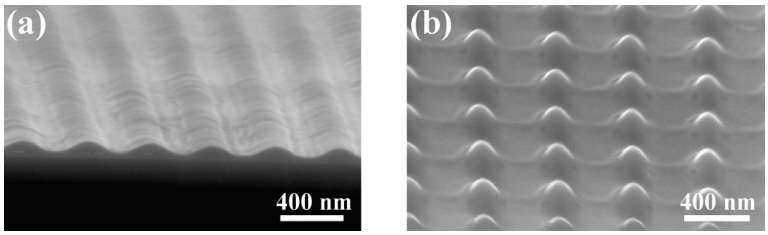

Figure 3.5. SEM images of (a) one-dimensional SRG and (b) two-dimensional SRG made by rotating the sample by 90 degrees between two subsequent exposures.

It is noticeable that, for obtaining a mask, a wet development of a photoresist is replaced by RIE of an azopolymer. The latter process is faster, simpler, and more controllable. Moreover, the substrate is usually further etched in the same RIE machine, which considerably saves the fabrication time.

If the substrate material is etched directly through a soft azopolymer mask, the etch profile turns out to be trapezoidal rather than rectangular [see Fig. 3.6(b)]. This is an inevitable effect that, however, can be beneficial if the structures to be fabricated contain trapezoidal or conical shapes, such as the ones in the moth-eye antireflection coatings [53, 54, 55, 56, 57]. If vertical walls are required for the etched pattern, one must use a hard mask. Such a mask, usually made of metal or oxide, can be fabricated with the help of a soft azopolymer mask.

Typical steps of an azopolymer-based interference lithography using an intermediate hard mask are shown in Fig. 3.7. A silicon wafer is first

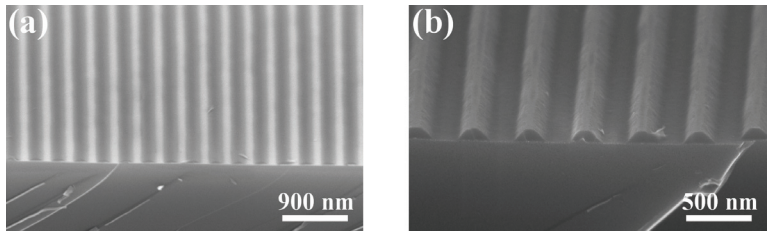

Figure 3.6. SEM images of (a) azopolymer mask and (b) silicon substrate etched through the azopolymer mask.

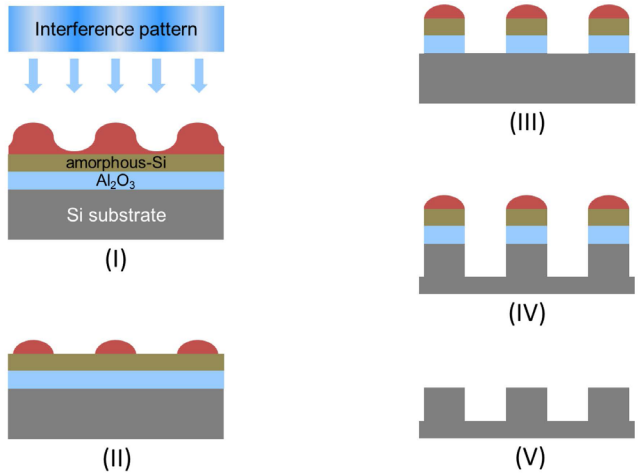

Figure 3.7. Schematic illustration of a fabrication process based on the use of an intermediate hard mask: (I) deposition of Al_2O_3 (5 nm), amorphous silicon (20 nm), azopolymer (100 nm), and SRG inscription, (II) partial etching of the polymer in O_2, (III) etching of amorphous silicon and Al_2O_3, (IV) dry etching of Si, and V) stripping the mask.

covered with a 5-nm thick layer of alumina, using an atomic layer deposition (ALD) process [98, 99, 100]. Alumina is chosen as one of the most effective masking materials for ICP-RIE of silicon, with the etch ratio being on the order of 10^6; and it is also very good for regular RIE. Next, a 20 nm thick layer of amorphous silicon (a-Si) is deposited on top of the alumina to act as an adhesion promoter for a layer of an azopolymer that is spin-coated onto the sample in the next step. Then, a soft azopolymer mask is fabricated (in the way described above) and the amorphous silicon is patterned through this mask with RIE. In the next step, the pattern is transferred from a-Si to alumina, using wet etching, which eventually yields a hard mask (Fig. 3.8). The obtained hard mask allows patterning silicon by using various etching conditions and parameters to obtain a variety of etching profiles (see Fig. 3.9).

To further develop the azopolymer-based interference lithography to-

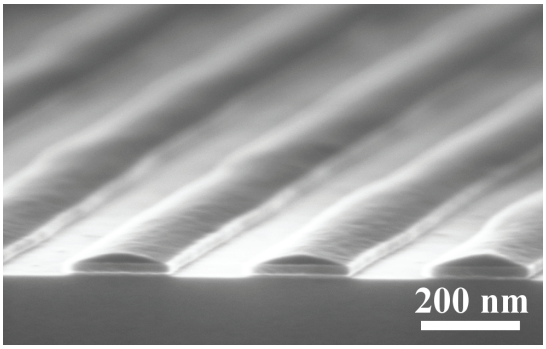

Figure 3.8. SEM image of a hard mask.

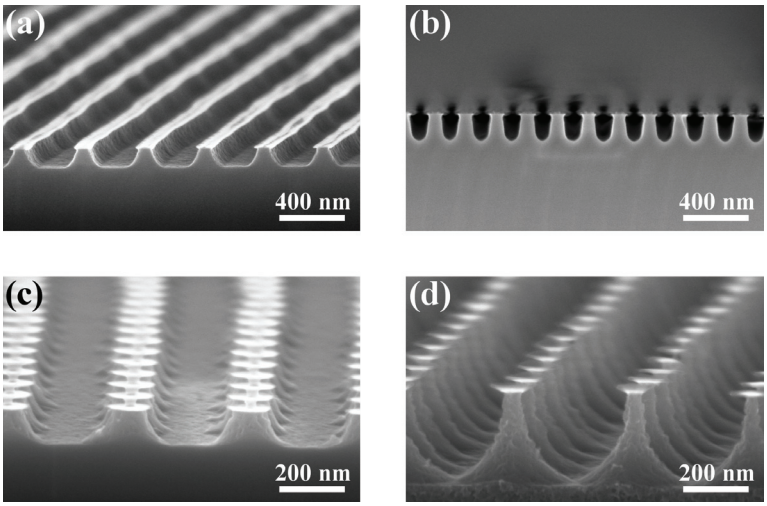

Figure 3.9. SEM images of silicon etched through a hard mask using different etching parameters.

wards wide technological applications, we have proposed and demonstrated an *all-dry etching* procedure for patterning bulk gold, silicon, glass and metal films on a dielectric substrate. The all-dry procedure is simple and fast, and it is very convenient to accomplish all the required etching steps without opening the RIE chamber. Moreover, creating a periodic mask pattern on a highly reflective substrate with some conventional holographic approach can be very challenging because of the already mentioned multiple reflections from the back and front surfaces of the sample. An example of a photoresist film patterned on a reflective substrate is shown in Fig. 3.10. The observed sinusoidal modulation of the mask's side walls is caused by standing waves of the reflected exposure light inside the photoresist. This destructive effect can be suppressed by exploiting special antireflection or absorbing coatings or by using extremely thin photoresist films (much thinner than a half of the exposure wavelength

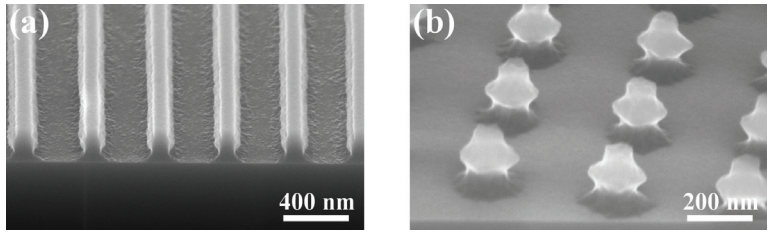

Figure 3.10. SEM images of photoresist masks with a standing-wave profile resulting from (a) single exposure and (b) double exposure.

in the material). However, the use of an antireflection coating can significantly complicate the fabrication process, and it is not always possible to find a material efficiently absorbing light at the wavelength of interest. Moreover, antireflection coatings are usually rather thick and they are nearly impossible to use when the pattern period is shorter than the coating thickness [107]. Too thin photoresist films, on the other hand, will drastically limit the maximum etch depth of the substrate. In contrast, patterning azopolymers is based on a spatially varying polarization state of the exposure light, and it is not very sensitive to the intensity modulation. This property makes azopolymers superior compared to photoresists, because high-quality SRGs can easily be created on highly reflective surfaces of, e.g., silicon or gold, which has been shown, both theoretically and experimentally in Publication II.

Many metals in general, and almost all noble metals in particular, do not form volatile chemical substances and, therefore, they cannot be dry-etched. However, they can easily be milled, e.g., by ions of argon, through a soft azopolymer mask. Furthermore, noble metals have a relatively low sputtering energy and a high sputtering yield, resulting in a high milling rate compared to that of the mask. We have successfully demonstrated in Publication II the possibility to transfer an azopolymer pattern to the surface of gold. We have also reported on patterning thin gold films and obtaining periodic arrays of gold nanodiscs. The film was completely removed from the areas that were not protected by the soft mask. Such metal patterns can be further used as hard etch masks for patterning an underlying dielectric or semiconductor material (see Fig. 3.11).

In the milling process, most of the argon ions collide with the surface of the sample at normal incidence. The collisions eject the atom from the surface. The prevailing direction of the atom ejection, as various statistical models show, can be just along the surface, which causes a significant amount of the material to be sputtered back onto the sample surface. This

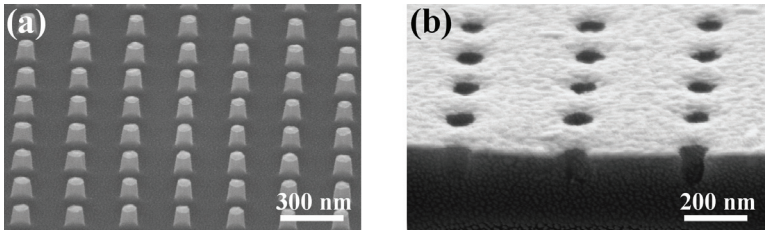

Figure 3.11. SEM images of (a) silicon and (b) glass surfaces etched through a hard mask made of gold. The etched glass surface was covered with 10 nm of gold for SEM imaging.

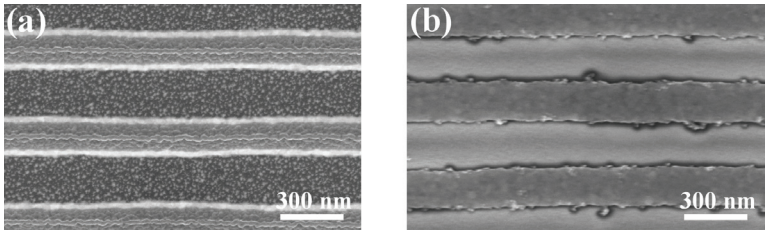

Figure 3.12. SEM images of a nanostructure (a) before (gold nanostructures are pale gray) and (b) after removal of the resputtered gold (gold nanostructures are dark gray).

resputtering contaminates the etched surface with tiny metal islands [see Fig. 3.12(a)]. To remove the resputtered metal, we add an intermediate sacrificial layer of alumina underneath the metal film to be patterned. Then, after patterning the metal, we dissolve the sacrificial layer in an acid, thus lifting-off the resputtered gold and obtaining nearly perfectly clean open areas of the mask [see Fig. 3.12(b)].

4. Photonic structures fabricated using azopolymer-based patterning

Periodic arrays of nanostructures fabricated using azopolymer-based lithography have a vast area of applications. They can be used as diffraction gratings [1], ultrathin polarizers [7], wave retarders [8, 9], moth-eye antireflection coatings [10], perfect absorbers, spectral filters [11], plasmonic sensors [13], etc. This section describes in detail the azopolymer-based fabrication of certain photonic structures and some of their properties.

4.1 Metal disc and hole arrays

Metal nanodisk and nanohole arrays exhibit pronounced surface-plasmon resonances at visible wavelengths [71, 148, 149] and can be used, e.g., to construct plasmonic filters [11] and sensors [150], to create SERS substrates [14], or to improve light absorption in solar cells [151], etc. In this thesis, an array of gold nanodiscs was fabricated and studied as described in Publication II. The array was manufactured on a polished glass substrate using a procedure that was briefly discussed in section 3.2. It is shown in Fig. 4.1 in more detail. First we deposit a 5-nm layer of alumina by using a Beneq TSF-500 atomic layer deposition machine. The deposition is done at 220 °C using trimethyl aluminum and water as precursors. Then we evaporate a 2-nm thick layer of titanium on the alumina. Titanium acts as an adhesion promoter between alumina and gold. After this, a 20-nm thick film of gold is deposited. Both metals are deposited in the same electron beam evaporator MASA IM-9912. The last step before etching is spin coating of the azopolymer [we used poly(Disperse Red 1 Acrylate) (pDR1A)] from a 2-w% solution in 1,2-dichloroethane. The coating is done within 30 s at a speed of 5000 RPM with a ramp of 3000 RPM. The deposited azopolymer film is then dried in an oven at 85° for approximately 2 hours in order to completely evaporate the solvent. In the next

step, we inscribe the surface relief grating. This is done by exposing the azopolymer film to an interference pattern, created in a Lloyd interferometer. We exploited a single mode argon laser tuned to the wavelength of 488 nm. The laser intensity was chosen to be 25 mW/cm^2. The interferometer was rotated to provide an incidence angle of 35°. The exposure time was set to 40 min for the first exposure and 20 min for the second orthogonal exposure if that was used. Next, the surface relief grating was partially etched by oxygen in a reactive ion etcher, Plasma Lab 80 Plus, Oxford Instruments and Plasma Technologies, to fabricate a soft mask. The etching parameters were as follows: O_2 flow – 40 standard cubic centimeters per minute (SCCM), O_2 pressure – 1.95 Pa, radio frequency (RF) generator power – 40 W and an etch time of 120 – 150 sec, depending on the task. For example, etching for 120 s yields an array of holes in the mask, while a 150 s etching time results in an array of disks.

Etching the sample starts with milling the gold and titanium through the azopolymer mask. This was done in the same RIE machine, but with the following process parameters for the argon gas: Ar flow – 25 SCCM, reactor pressure – 1.05 Pa, RF generator power – 100 W, and an etching time between 3 min and 6 min. To avoid sample overheating and consequent mask meltdown, the milling was done in 30-sec steps with 2 min cooling intervals. After this step, the resputtered gold was lifted off via dissolving the sacrificial alumina layer in aluminium etchant solution BASF PS80-16-04(65) at 50 °C for 15 min. The choice of alumina for the sacrificial layer was based on its excellent etching selectivity and the fact that Al_2O_3 is optically transparent. The latter property is important if the sample is to be used in applications in optics. As a last step we stripped the azopolymer mask by 6-min exposure of the sample to O_2 plasma (in a PVA TePla Microwave Plasma Systems 400; the machine was set to O_2 flow of 1700 ml/min, Ar flow of 50 ml/min, RF power of 1000 W and chamber pressure of 4.7 mbar). To improve plasmonic properties of the fabricated array the sample was annealed in nitrogen for 20 min at 400 °C. SEM images of the fabricated nanohole and nanodisk arrays are shown in Fig. 4.2. The average diameter of the nanodisks was 250 nm and the pattern period 410 nm. The holes and disks are obtained using different masks, as described above.

The optical properties of the fabricated nanodisc array were studied by measuring the array's transmission and reflection spectra [see Fig. 4.3]. The measurements were done with the help of a Perkin Elmer Lambda

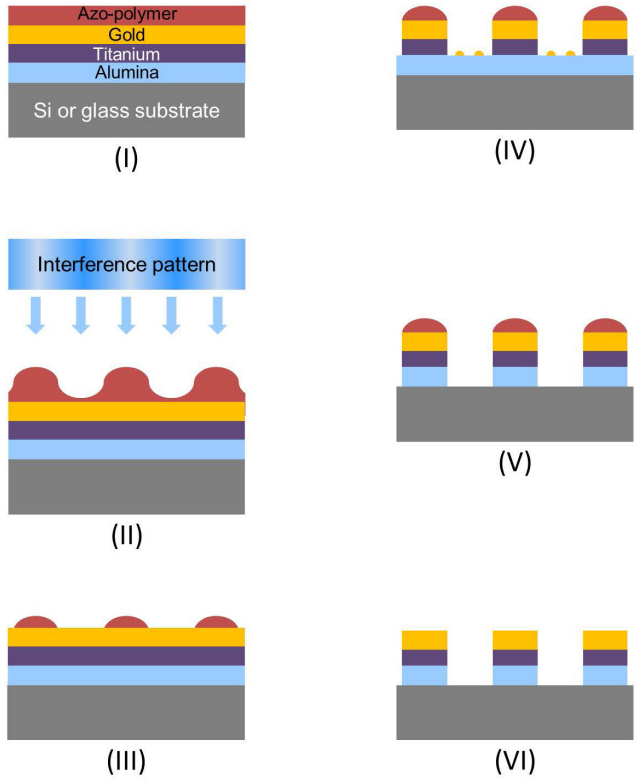

Figure 4.1. Fabrication of periodic plasmonic structures using azopolymer-based lithography: (I) Deposition of alumina (5 nm), titanium (2 nm), gold (20 nm) and azo-polymer (100 nm), (II) Inscription of the SRG, (III) Partial etching of the polymer in O_2, (IV) milling the gold and titanium by Ar, (V) lift off the the resputtered gold by etching of the alumina, (VI) stripping the azo-polymer mask.

950 spectrophotometer. The sample transmittance considerably drops around the wavelength of 850 nm due to a surface plasmon resonance in the disks. Simultaneously, the reflectance shows a peak at these wavelengths. This peak is broad, spanning from ca 700 nm to 1100 nm. The experimental spectra agree well with the corresponding numerically simulated spectra [see Fig. 4.3]. The calculations were done for an array of identical perfect nanodiscs [152]. The experimental peaks are somewhat wider, presumably due to small variations in the geometry of the individual disks and a residual contamination of the substrate.

The obtained metal nanodisc and nanohole arrays can also be used as masks for dry-etching the substrate (Fig. 4.4). We etched silicon and glass through such masks using the same RIE machine as in the previous examples. Silicon was etched under the following conditions: CF_4 flow of 45 SCCM, CHF_3 flow of 45 SCCM, reactor pressure of 1.33 Pa, RF gen-

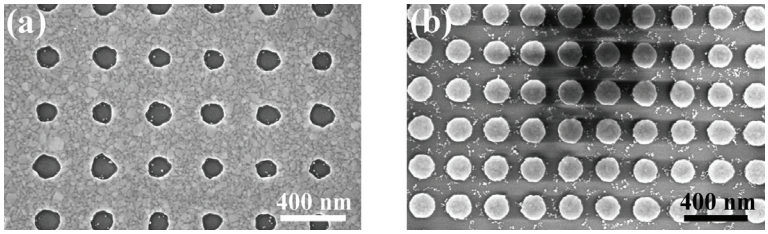

Figure 4.2. SEM images of (a) a nanohole array and (b) a nanodisk array.

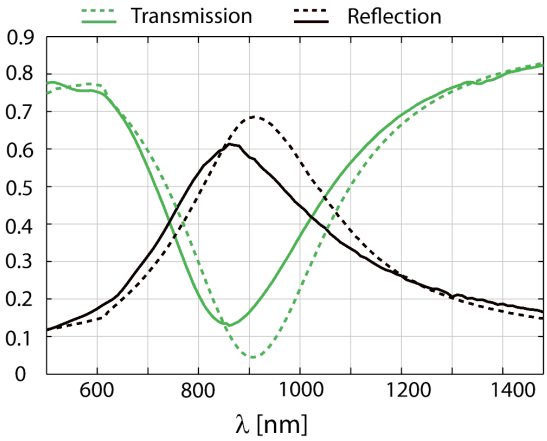

Figure 4.3. The transmission and reflection spectra of the gold nanodisc array. Solid lines – experimentally measured spectra, dashed lines – calculated spectra.

erator power of 40 W, and etching time of 17 min (the etch rate was ca. 5 nm/min). The glass substrates were etched under different conditions, which were as follows: CF_4 flow of 20 SCCM, CHF_3 flow of 60 SCCM, RF generator power of 50 W, reactor pressure of 4.00 Pa, and etching time of 20 min (the etch rate was also about 5 nm/min). The slow etch rates were chosen intentionally for fine control of the pattern depth. Etching of silicon resulted in vertical side walls of the etched profiles [see Fig. 4.4(a)]. Etching glass through a gold mask yielded conical side-wall surfaces [see Fig. 4.4(b)] due to the slow etching of the mask edges. In fact, that is exactly what would be needed for creating moth-eye antireflection coatings. If, on the other hand, vertical side walls are of interest, gold should be replaced with another masking material, such as silver or chromium. At the end, the metal masks were removed by rinsing the sample in diluted aqua regia (3 parts of 37 % HCl, 1 part of 70 % HNO_3, and 2 parts of H_2O).

An alternative nanofabrication approach, in which metal is deposited on top of an inscribed SRG and then milled at a large angle is introduced in Publication IV. The method is facile and scalable, allowing fabrication

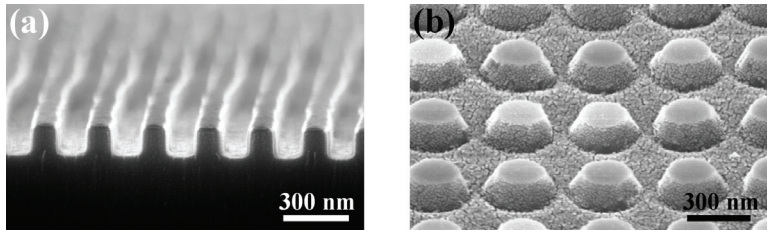

Figure 4.4. SEM images of etched (a) silicon nanoridges and (b) glass nanocones. The gold mask is still present. The glass array in (b) was additionally covered with a thin layer of gold for SEM imaging.

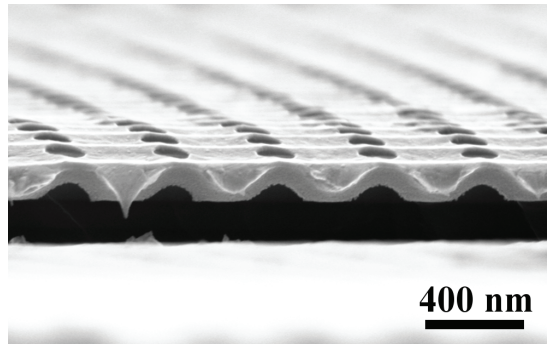

Figure 4.5. SEM image of a tapered nanohole array.

of periodic arrays of unique threedimensional subwavelength-sized structures such as tapered holes and pyramidically shaped subwavelength-sized particles. The method allows fabricating highly uniform arrays with tunable lattice parameters and dimensions over large sample areas. The process flow of the technique is as follows: First, a transparent substrate is spin-coated with an azopolymer and an SRG is inscribed. In the next step, a gold film is evaporated on top of the grating at normal incidence. This results in a surface topology of the metal film which repeats that of the SRG. Finally, the metal film is milled with an argon ion beam incident at a large incidence angle onto the SRG surface. Because of this glancing angle of incidence, the hills of the gold SRG obscure the grating valleys. Thus the argon beam can only mill off the top parts of the grating. This process yields a metal film with holes (Fig. 4.5). A longer milling time would result in a periodic array of nanoislands in the dimples of the SRG. The obtained, slightly tapered holes were observed to show sharper plasmon resonances, which can be beneficial for construction of plasmonic sensors [13, 150]. Moreover, the presence of the photosensitive azopolymer layer underneath the gold opens up the possibility to tune the optical response of the array.

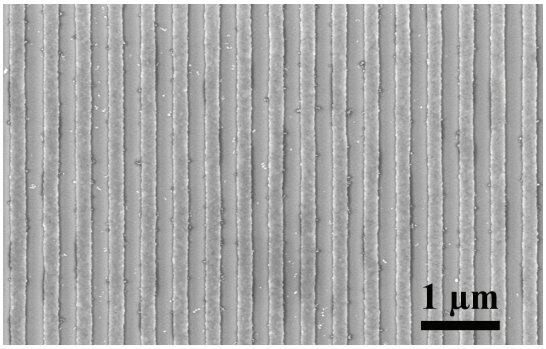

Figure 4.6. A SEM image of a wire-grid polarizer consisting of gold stripes on glass.

4.2 Nanogrid polarizers and waveplates

Nanogrid polarizers[43, 44, 7] and wave retarders [8, 48] have many potential and already existing applications in optics, especially in imaging systems and displays. Working on topics of Publication II, we have fabricated a number of metal wire-grid polarizers. A SEM image of one of them is shown in Fig. 4.6. The fabrication procedure was essentially the same as the one used to create the metal nanodisc and nanohole arrays. The exception is that the azopolymer film was exposed only to a single interference fringe pattern. The device consists of periodically arranged thin stripes of gold on a glass substrate. The pattern period is 400 nm. The thickness of gold on the substrate is about 40 nm. The polarizer transmits light polarized perpendicularly to the stripes and reflects the orthogonal component polarized along the stripes.

Reflective metal nano-grid wave plates have a somewhat similar structure and operational principle. They are flat metal samples with a periodic pattern of rectangular nanogrooves on the surface [48]. Along with a long range periodicity it is required that the grooves have vertical side walls. Furthermore, since the pattern period must be small compared with the wavelength and the groove depth must be on the order of $\lambda/4$, the pattern aspect ratio is often quite high. Such structures are rather difficult to manufacture on a large surface area by using conventional nanofabrication techniques. As has been already mentioned, deep anisotropic dry etching is nearly impossible for noble metals as they do not form any suitable volatile chemical compositions. Wet etching, on the other hand, is isotropic for polycrystalline metals, which makes it impossible to etch thermally evaporated metal films and obtain vertical side walls. Ion milling is also unsuitable for creation of deep rectangular grooves,

because of uncontrollable redeposition of metal atoms (ejected from the sample during the milling) onto the side walls of the pattern.

A novel fabrication approach (that led to Publication III) has been developed in the course of this work on metal nano-grid wave plates. The fabrication process is schematically shown in Fig. 4.7. We start by fabricating a rectangular groove pattern in silicon, with a geometry that is complementary to the designed geometry of the metal wave plate. This is done by etching a silicon substrate through a hard gold mask created by using the azopolymer-based interference lithography. Then, we deposit a 5-nm layer of alumina, using ALD, and a monolayer of trichloromethylsilane (CH_3Cl_3Si), with the help of physical vapor deposition. Alumina is intended to decrease adhesion of gold to the substrate and, in addition, it is used to adjust the width of the trenches in the substrate. In the last step we evaporate a thick layer of gold onto the sample at normal incidence. The thickness of the layer must be larger than the desired groove depth (also in order to completely cover the pattern, which is important in view of the next step). A glass plate is then glued to the metal with UV-curable epoxy; the epoxy is illuminated through the glass. In the next step we decouple the glued metal from the template and obtain the desired metal structure. The fabricated stamp can be used multiple times. Figure 4.8 shows SEM images of such a silicon stamp and a reflective nano-grid wave plate created using this stamp. The pattern period is 260 nm, the ridge width is 100 nm, and the trench depth is 210 nm. The area of the pattern is about 1 cm^2.

Optical properties of the fabricated device were studied using the experimental setup depicted in Fig. 4.9. In this setup, broadband light from a tungsten lamp is collimated, polarized with a linear broadband polarizer, and incident on the sample at an angle of about 9°. This angle is small, and as was verified by both numerical calculations and measurements, it yields optical spectra, which are indistinguishable from those obtained at normal incidence. The transmission axis of the polarizer was oriented at 45° to the grooves. The reflected light was analyzed with another broadband polarizer (analyzer) and a fiber-coupled spectrometer. At first, we measured the reflection spectrum of a planar film of gold as a reference. The measurement was done at the orientation of the analyzer providing the maximum transmission. This spectrum was then subtracted from the measured reflection spectra of the sample to eliminate reflection losses at the polarizers and the sample's material factor (the contribution of gold).

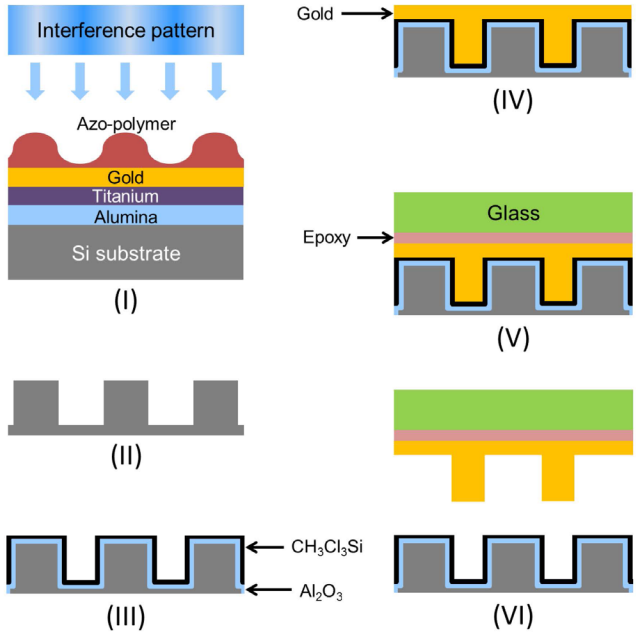

Figure 4.7. Fabrication steps used to create metal nano-grid wave plates.

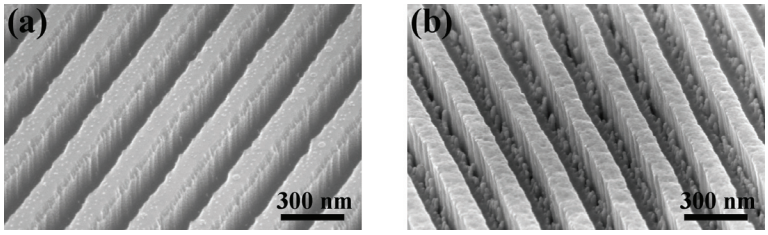

Figure 4.8. SEM images of (a) the stamp and (b) a reflective wave plate.

The system transmission spectra were recorder for the full 360° rotation of the analyzer in steps of 5°. The measured transmittance, T, of the system as a function of the analyzer angle α is shown for several particular wavelengths in Fig. 4.10(a). It can be seen that at the wavelength of 604 nm, the transmission of the system does not depend on the analyzer angle. This means that the wave plate converts the incident linearly polarized light into circularly polarized and thus acts as a quarter-wave plate. The observed transmittance of 0.4 at this wavelength indicates that c.a. 20 % of light power is lost, presumably by being absorbed in the grooves and scattered at fabrication imperfections.

At the wavelength of 997 nm, the reflectance reaches zero when the transmission axes of the polarizers are essentially parallel to each other, conforming that the device acts as a half-wave plate. At crossed polarizers, the transmittance attains the maximum value, as it should. Again,

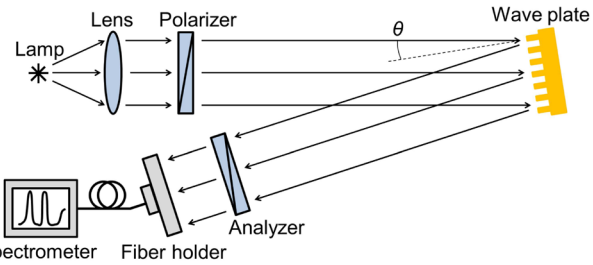

Figure 4.9. Experimental setup for optical characterization of the fabricated gold nano-grid wave plate.

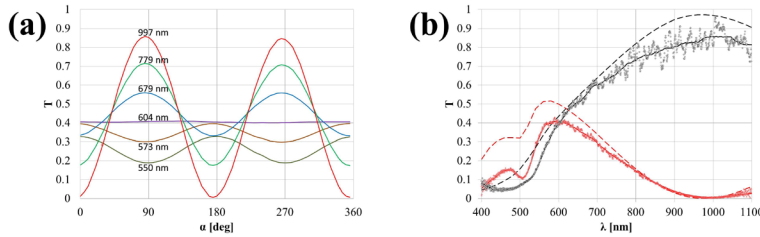

Figure 4.10. (a) The system transmittance measured at several wavelengths as a function of the orientation angle α of the analyzer. (b) The spectra measured when the axes of the polarizer and analyzer are parallel (black curves) and perpendicular (red curves) to each other; the corresponding theoretical curves are shown by the dashed lines.

the reflection is not perfect due to absorption and scattering in the grooves. The measured transmittance spectra of the system are shown in Fig. 4.10(b) for two particular orientation angles of the analyzer of 0° (red curve) and 90° (black curve). These graphs clearly show the quarter- and half-wave operations of the wave plate at 604 nm and 997 nm, respectively. The experimental results are in good agreement with the results of numerical calculations performed for the case of ideally flat surfaces of the grooves (see the dashed curves in the figure). The measured transmittance is lower than the theoretical one especially for the polarization component which is perpendicular to the grooves. This implies that optical losses take place mainly inside the trenches.

The proposed nanofabrication technique allows fast production of periodically surface-patterned metal samples. The patterns can easily be created on a large surface area, have vertical walls and contain high-aspect-ratio nanostructures. The fabricated reflective nano-grid wave plate is an example of optical elements that can be obtained using this method. An important advantage of such nanostructured elements over their conventional (micro- and macrostructured) counterparts is that the former

can have a wider operation band, and they can be considerably thinner. A wire-grid polarizer and a moth-eye antireflection coating are two more examples of such devices.

4.3 Nanopillar arrays and SERS substrates

Periodic arrays of nano- and micropillars have widespread technological applications, ranging from photonic crystals [2, 3, 4, 5, 6] to chemical and biological sensors [13, 150], including their use as substrates for surface enhanced Raman spectroscopy [14]. We have extended our azopolymer-based interference lithography towards fabrication of such periodic arrays of nanopillars and applied the technique to fabricate SERS substrates. The results of this work are presented only in this compendium. The fabrication process is shown in Fig. 4.11. We start with coating a silicon substrate with a stack of 1.5-nm thick film of titanium, 40-nm film of gold and 100-nm layer of azopolymer. Then a one- or two-dimensional surface relief grating is inscribed and, as previously, etched in oxygen RIE to create a soft mask. Next we pattern the gold using argon milling in RIE through the soft mask. The formed hard mask is then used for further anisotropic etching of the wafer with RIE. After this we strip the mask in diluted aqua regia and use ALD to cover the substrate with a 7 nm thick layer of alumina. This layer is used to decrease adhesion of silver that is deposited next. The deposition of silver is done onto the side walls of the pillars from two opposite sides at a large deposition angle. This results in formation of pairs of silver islands on the pillars. Then we anisotropically mill both the silver and alumina with argon RIE to remove these materials from the top surfaces of the pillars and the surface of the sample between them. This yields pairs of silver nanocrescents around the pillars (see Fig. 4.12). In the next step the crescents are transformed into nanospheres by annelaling the sample for 20 min in nitrogen at 400 °C. These nanospheres are then used as a mask to etch silicon. A periodic array of nanopillar pairs obtained in this way is shown in Fig. 4.12. Next we strip the silver and evaporate a 1.5 nm thick film of titanium and a 100 nm thick film of gold onto the pillars' top surfaces. The evaporation is performed at a very low evaporation rate (ca 0.5 Å/sec), promoting a liquid-like behavior of the metal, to form nanospheroids instead of discs. Finally, to improve the plasmonic properties of the metal, we anneal the sample for 20 min in nitrogen at 400 °C

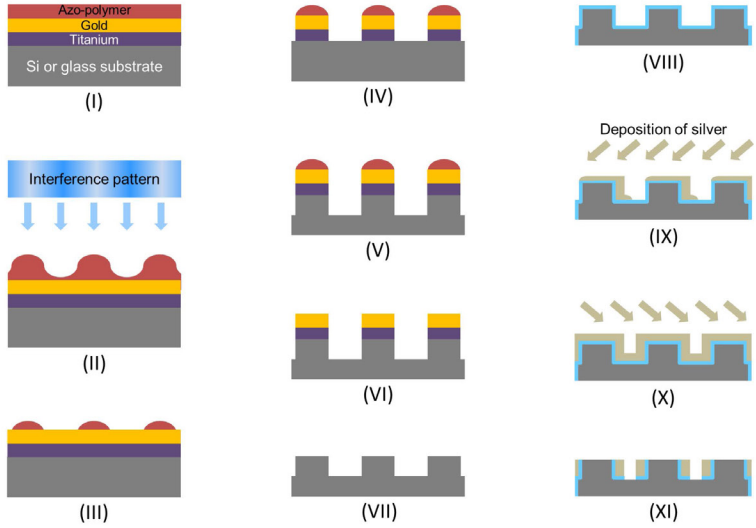

Figure 4.11. Fabrication of nanopillar arrays.

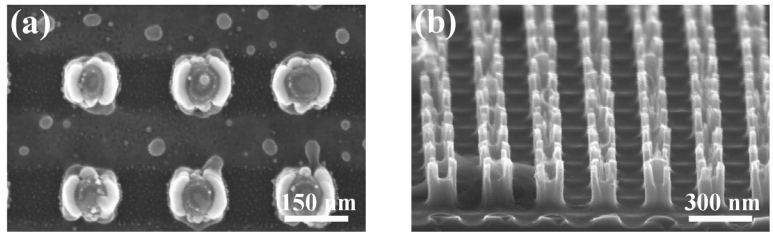

Figure 4.12. SEM images of the fabricated nanopillar arrays.

SERS substrates fabricated using this technique were observed to provide a high surface-averaged SERS enhancement factor ($> 10^7$ for thioglycerol). Furthermore, since large surface areas can be patterned, the technique is very promising in view of possible mass production of the SERS substrates.

5. Summary and outlook

The main result of the work presented in this thesis is the development of versatile nanofabrication techniques for manufacturing periodic arrays of various optical nanoelements. The developed technique is simpler and faster than the standard photoresist-based interference lithography, and it is suitable for patterning not only transparent and absorptive, but also highly reflective materials, such as silver and gold surfaces.

In the introduced interference lithography, conventional photoresists are replaced with azobenzene-functionalized polymers. These polymers are insensitive to stray light as well as to temperature and humidity fluctuations. In addition, creation of azo-polymer masks does not require any wet processing, which drastically simplifies and speeds up the fabrication cycle. Moreover, since azo-polymers are tolerant to overexposure, complex mask patterns can easily be created by applying sequentially multiple interference patterns, e.g., with different orientations and/or periods.

We have further developed our nanofabrication technique to facilitate surface patterning of metals and dielectrics. We have experimentally demonstrated the creation of a large-area nanodisk array made of gold on glass. Such patterns can be used as plasmonic sensors and spectral filters. Introducing a sacrificial layer of alumina solved the problem of contamination of the sample by resputtered metal during the etching. The fabricated nanodisk array was also used as an etch mask to pattern glass substrates in order to obtain a periodic array of glass nanocones. Such a nanocone array can be used as a moth-eye antireflection coating.

Using the azo-polymer based interference lithography, it is possible to create a hard mask which repeats the azo-polymer SRG pattern. The hard mask allowed us to etch deeper into silicon. We have used this approach to fabricate reflective metal nanogrid wave plates. The wave plates were proven to work as high-quality quarter- and half-wave plates within a

wide spectral range.

An alternative means to produce large-area nanohole arrays by making use of azo-polymers was demonstrated by depositing a gold film on an azo-polymer SRG pattern and cutting the top parts of the film with argon milling at a glancing incidence angle. This technique preserves the underlying azo-polymer, opening up a new possibility to tune the optical response of the structure through an interplay between surface-plasmon excitations in the perforated film and the photosensitivity of the polymer.

The presented nanofabrication methods can be further developed towards more sophisticated patterns and a broader range of materials. As an example, we have combined the azo-polymer lithography with a nanopatterning technique based on self-assembly of silver nanoislands and created periodic arrays of nanopillar pairs with gold caps. These arrays exhibited a very high SERS enhancement factor. We anticipate that in the future it will be possible to create even more complicated nanostructures, including, e.g., three-dimensional metamaterials and photonic crystals by using azo-benzene-based nanofabrication methods similar to those described in this thesis.

Bibliography

[1] E. Hecht, *Optics* (Addison Wesley, San Francisco, 2002), pp.476-485.

[2] M. Campbell, D. N. Sharp, M. T. Harrison, R. G. Denning, A. J. Turberfield, Nature **404** 53 (2000).

[3] J. Valentine, S. Zhang, T. Zentgraf, E. Ulin-Avila, D. A. Genov, G. Bartal, X. Zhang, Nature **455**, 376 (2008).

[4] G. I.N. Waterhouse, M. R. Waterland, Polyhedron **26**, 356 (2007).

[5] W. Bogaerts, V. Wiaux, D. Taillaert, s. Beckx, B. Luyssaert, P. Bienstman, R. Baets, IEEE Journal in Quantum Electronics **8**, 928 (2002).

[6] Z. Dang, M. BH Breese, G. Recio-Sanchez, S. Azimi, J. Song, H. Liang, A. Banas, V. Torres-Costa, R. J. Martín-Palma, Nanoscale Research Letters **7** 416 (2012).

[7] H. Tamada, T. Doumuki, T. Yamaguchi, S. Matsumoto, Opt. Let. **22**, 419 (1997).

[8] S. L. Wadsworth, G. D. Boreman, Optt. Express **19**, 10604 (2011).

[9] B. Paivanranta, N. Passilly, J. Pietarinen, P. Laakkonen, M. Kuittinen, J. Tervo, Opt. Express **16**, 16334 (2008).

[10] H. K. Raut, V. A. Ganesh, A. S. Nairb, S. Ramakrishna, Energy Environ. Sci. **4**, 3779 (2011).

[11] S. Enoch, R. Quidant, G. Badenes, Opt. Express **12**, 3422 (2004).

[12] D. Dai, L. Liu, L. Wosinski, S. He, Electron. Lett. **42**, 400 (2006).

[13] R. Adato, A. A. Yanik, J. J. Amsden, D. L. Kaplan, F. G. Omenetto, M. K. Hong, S. Erramilli, H. Altug, Proc. Natl. Acad. Sci. USA **106**, 19227 (2009).

[14] C. Cheng, B. Yan, S. M. Wong, X. Li, W. Zhou, T. Yu, Z. Shen, H. Yu, H. J. Fan†, ACS Appl. Mater. Interfaces **2**, 1824 (2010).

[15] X.-M. Li, D. Reinhoudt M. Crego-Calama, Chem. Soc. Rev. **36**, 1350 (2007).

[16] J.-Y. Shiu, C.-W. Kuo, P. Chen, C.-Y. Mou, Chem. Mater. **16**, 563 (2004).

[17] A. Tuteja, W. Choi, M. Ma, J. M. Mabry, S. A. Mazzella, G. C. Rutledge, G H. McKinley, R. E. Cohen, Science **318**, 1618 (2007).

[18] T. Xu, Y.-K. Wu, X. Luo, L. J. Guo, Nat. Commun. **1**, 59 (2010).

[19] N. Takeshima, Y. Narita, S. Tanaka, Y. Kuroiwa, K. Hirao, Opt. Lett. **30** 352 (2005).

[20] F. He, H. Sun, M. Huang, J. Xu, Y. Liao, Z. Zhou, Y. Cheng, Z. Xu, K. Sugioka, K. Midorikawa, Appl. Phys. A **97** 853(2009).

[21] J. E. Harvey, A. Krywonos, D. Bogunovic, J. Opt. Soc. Am. A **23** 858 (2006).

[22] K. O. Hill, G. Meltz, J. Lightwave Technol. **15** 1263 (1997).

[23] K. O. Hill, Y. Fujii, D. C. Johnson, B. S. Kawasaki, Appl. Phys. Lett. **32** 647 (1978).

[24] B. S. Kawasaki, K. O. Hill, D. C. Johnson, Y. Fujii, Opt. Lett. **3** 66 (1978).

[25] E. Yablonovitch, Nato Science Series B **340** 885 (1995).

[26] K. M. Ho, C. T. Chan, C. M. Soukoulis, Phys. Rev. Lett. **65** 3152 (1990).

[27] M. Notomi, Phys. Rev. B **62** 10696 (2000).

[28] B. E. A. Saleh, M. C. Teich (2001) Photons and atoms, in Fundamentals of Photonics, John Wiley & Sons, Inc., New York, USA.

[29] Y.J Rao, Opt. Laser. Eng. **31** 297 (1999).

[30] J. D. Joannopoulos, P. R. Villeneive, S. Fan, Nature **386** 143 (1997).

[31] A. Mekis, J. C. Chen, I. Kurland, S. Fan, P. R. Villeneuve, J. D. Joannopoulos, Phys. Rev. Lett. **77**, 3787 (1996).

[32] M. Notomi, K. Yamada, A. Shinya, J. Takahashi, C. Takahashi, I. Yokohama, Phys. Rev. Lett. **87**, 253902 (2001).

[33] Y. A. Vlasov, M. O'Boyle, H. F. Hamann, S. J. McNab, Nature **438**, 65 (2005).

[34] Z. Lu, S. Shi, J. A. Murakowski, G. J. Schneider, C. A. Schuetz, D. W. Prather, Phys. Rev. Lett. **96**, 173902 (2006).

[35] D. W. Prather, S. Shi, J. Murakowski, G. J. Schneider, A. Sharkawy, C. Chen, B. Miao, R. Martin, J. Phys. D: Appl. Phys. **40**, 2635 (2007).

[36] G. Magno, M. Grande, A. Monmayrant, F. Lozes-Dupuy, O. Gauthier-Lafaye, G. Calo, V. Petruzzelli, J. Opt. Soc. Am. B, **31**, 355 (2014).

[37] J. Witzens, M. Loncar, A. Scherer, IEEE J. Sel. Top. Quant. Electron. **8**, 1246 (2002).

[38] E. Cubukcu, K. Aydin, E. Ozbay, S. Foteinopoulou, C. M. Soukoulis, Nature **423**, 604 (2003).

[39] P. V. Parimi, W. T. Lu, P. Vodo, S. Sridhar, Nature **426**, 404 (2003).

[40] D. R. Smith, J. B. Pendry, M. C. K. Wiltshire, Science **305**, 788 (2004).

[41] R. A. Shelby, D. R. Smith, S. Schultz, Science **292**, 77 (2001).

[42] J. J. Baumberg, N. M. B. Perney, M. C. Netti, M. D. C. Charlton, M. Zoorob, G. J. Parker, Appl. Phys. Lett. **85**, 354 (2004).

[43] G. P. Nordin, J. T. Meier, P. C. Deguzman, M. W. Jones, J. Opt. Soc. Am. A, **16**, 1168 (1999).

[44] C. Pentico, E. Gardner, D. Hansen, R. Perkins, SID Int. Symp. Dig. Tec. **32**, 1278 (2001).

[45] M. Honkanen, V. Kettunen, M. Kuittinen, J. Lautanen, J. Turunen, B. Schnabel, F.Wyrowski, Appl. Phys. B **68**, 81 (1999).

[46] T. Weber, T. Kasebier, E.-B. Kley, A Tunnermann, Opt. Lett. **36**, 445 (2011).

[47] H. Schift, A. Kristensen 297 (2010) Subwavelength metal-strip gratings, in handbook of nanotechnology, Springer, New York, USA.

[48] Y. Pang and R. Gordon, Opt. Express**17** 1271 (2009).

[49] Lord Rayleigh, Proc. London Math. Soc. **XI**, 51 (1880)

[50] J. A. Dobrowolski, D. Poitras, P. Ma, H. Vakil, M. Acree, Appl. Opt. **14**, 3075 (2002).

[51] Y.-J. Lee, D. S. Ruby, D. W. Peters, B. B. McKenzie, J. W. P. Hsu, Nano Lett. **8**, 1501 (2008).

[52] L. Zhang , Y. Li , J. Sun, J. Shen, Langmuir **24**, 10851 (2008).

[53] S.J. Wilson, M.C. Hutley, Opt. Acta **29**, 993 (1982).

[54] C.-H. Sun, P. Jiang, B. Jiang, Appl. Phys. Lett. **92**, 061112 (2008).

[55] Y.-F. Huang, S. Chattopadhyay, Y.-J. Jen, C.-Y. Peng, T.-A. Liu, Y.-K. Hsu, C.-L. Pan, H.-C. Lo, C.-H. Hsu, Y.-H. Chang, C.-S. Lee, K.-H. Chen, L.-C. Chen, Nat. Nanotechnol. **2**, 770 (2007).

[56] Q. Chen, G. Hubbard, P. A. Shields, C. Liu, D. W. E. Allsopp, W. N. Wang and S. Abbott, Appl. Phys. Lett. **94**, 263118 (2009).

[57] W. H. Southwell, J. Opt. Soc. Am. A **8**, 549 (1991).

[58] Y. Li, J. Zhang, S. Zhu, H. Dong, Z. Wang, Z. Sun, J. Guoa, B. Yang, J. Mater. Chem. **19**, 1806 (2009).

[59] L. G. Schulz, F. R. Tangherlini, J. Opt. Soc. Am. **44**, 362 (1954).

[60] M. Suffczynski, Phys. Rev. **177**, 663 (1960).

[61] P. B. Johnson, R. W. Christy, Phys. Rev. B **6**, 4370 (1972).

[62] J. B. Pendry, L. Martin-Moreno, F. J. Garcia-Vidal, Science **305**, 847 (2004).

[63] S. Lal, S. Link, N. J. Halas, Nature Photonics **1**, 641 (2007).

[64] K. L. Kelly , E. Coronado , L. L. Zhao, G. C. Schatz, J. Phys. Chem. B **107**, 668 (2003).

[65] C. Sonnichsen, T. Franzl, T. Wilk, G. von Plessen, J. Feldmann, O. Wilson, P. Mulvaney, Phys. Rev. Lett. **88**, (2002).

[66] J. A. Creighton, C. G. Blatchford, M. G. Albrecht, J. Chem. Soc. Faraday Trans. **2**, 790 (1979).

[67] A. Otto, Zeitschrift für Physik **216** 398, (1968).

[68] W. L. Barnes, A. Dereux, T. W. Ebbesen, Nature **424**, 824 (2003).

[69] D. Sarid, Phys. Rev. Lett. **47**, 1927 (1981).

[70] A. Krishnan, T. Thio, T.J. Kim, H.J. Lezec, T.W. Ebbesen, P.A. Wolff, J. Pendry, L. Martin-Moreno, F.J. Garcia-Vidal, Opt. Commun. **200**, 1 (2001).

[71] S. Eustis, M, A. El-Sayed, Chem. Soc. Rev. **34**, 209 (2005).

[72] L. M. Liz-Marzan, Langmuir **22**, 32 (2006).

[73] B. Lamprecht, G. Schider, R. T. Lechner, H. Ditlbacher, J. R. Krenn, A. Leitner, and F. R. Aussenegg, Phys. Rev. Lett. **84**, 4721 (2000).

[74] S. Link, M. A. El-Sayed, J. Phys. Chem. B **103**, 4212 (1999).

[75] P. K. Jain, X. Huang, Ivan H. El-Sayed, M. A. El-Sayed, Plasmonics /textbf2, 107 (2007).

[76] D. A. Genov, A. K. Sarychev, V. M. Shalaev, A. Wei, Nano Lett. **4**, 153 (2004).

[77] S. Zou, G. C. Schatz, Chem. Phys. Lett. **403**, 62 (2005).

[78] H. Wang, C. S. Levin, N. J. Halas, J. Am. Chem. Soc. **127**, 14992 (2005).

[79] A. Campion, P. Kambhampati, Chem. Soc. Rev. **27**, 241 (1998).

[80] C. E. Talley,J. B. Jackson, C. Oubre, N. K. Grady, C. W. Hollars, S. M. Lane, T. R. Huser, P. Nordlander, N J. Halas, Nano Lett. **5**, 1569 (2005).

[81] J. B. Jackson, N. J. Halas, PNAS **101**, 17930 (2004).

[82] N. Felidj, J. Aubard, G. Levi, J. R. Krenn, A. Hohenau, G. Schider, A. Leitner, F. R. Aussenegg, Appl. Phys. Lett. **82**, 3095 (2003).

[83] S. Nie, S. R. Emory, Science **275**, 1102 (1997).

[84] K. Kneipp, Y. Wang, H. Kneipp, L. T. Perelman, I. Itzkan, R. R. Dasari, M. S. Feld, Phys. Rev. Lett. **78**, 1667 (1997).

[85] K. Kneipp, H. Kneipp, I. Itzkan, R. R. Dasari, M. S. Feld, Chem. Rev. **99**, 2957 (1999).

[86] Y. C. Cao, R. Jin, C. A. Mirkin, Science **297**, 1536 (2002).

[87] S. Franssila, *Intoroduction to microfabrication* (A John Willey and Sons, Chichester, UK, 2010).

[88] M. J. Madou, *Fundamentals of microfabrication and nanotechnology* (CRC Press, Boca Raton, USA, 2012).

[89] M. Kufner, S. Kufner, *Micro-optics and lithography*, (VUB Press, Brussels, Belgium, 1997).

[90] Process start-up and optimization, (MicroChemicals GmbH, 2005, http://microchemicals.net/technical_information/litho_process_startup.pdf).

[91] Exposure of photoresist, (MicroChemicals GmbH, 2010, http://microchemicals.net/technical_information/exposure_photoresist.pdf).

[92] Greyscale lithography with photoresists, (MicroChemicals GmbH, 2009, http://microchemicals.net/technical_information/greyscale_lithography.pdf).

[93] Laser exposure of photoresist, (MicroChemicals GmbH, 2010, http://microchemicals.net/technical_information/laser_exposure_photo_resist.pdf).

[94] Resists, developers and removers, (MicroChemicals GmbH, 2009, http://microchemicals.net/technical_information/resists_developers_removers.pdf).

[95] J. A. Thornton, Ann. Rev. Mater. Sci. **7**, 239 (1977).

[96] P. J. Kelly, R.D. Arnell, Vacuum **56**, 159 (2000).

[97] L. Holland, *Vacuum deposition of thin films*, (Chapman and Hall, UK, 1956).

[98] S. M. George, Chem. Rev. **110**, 111 (2010).

[99] R. L. Puurunen, J. Appl. Phys. **97**, 121301 (2005).

[100] M. Leskela, M. Ritala, Thin solid films **409**, 138 (2002).

[101] K. L. Choy, Prog. Mater. Sci. **48**, 57 (2003).

[102] W. A. Bryant, J. Mater. Sci. **12**, 1285 (1977).

[103] A. F. Lasagni, T. Roch, D. Langheinrich, M. Bieda, A. Wetzig, Physics Procedia **12**, 214 (2011).

[104] Q. Xie, M.H. Hong, H.L. Tan, G.X. Chen, L.P. Shi, T.C. Chong, J. Alloys Compd. **449**, 261 (2008).

[105] N. Feth, C. Enkrich, M. Wegener, Opt. Express **15**, 501 (2007).

[106] J.-M. Park, K.S. Nalwa, W. Leung, K. Constant, S. Chaudhary, K.-M. Ho, Nanotechnology **21**, 215301.2 (2010).

[107] H. van Wolferen, L. Abelmann, in: T.C. Hennessy (Ed.), Lithography: Principles, Processes and Materials (Nova Science Publishers Inc., New York NY, 2011).

[108] H.C. Guo, D. Nau, A. Radke, X.P. Zhang, J. Stodolka, X.L. Yang, S.G. Tikhodeev, N.A. Gippius, H. Giessen, Appl. Phys. B. **81**, 271 (2005).

[109] A.A. Tseng, K. Chen, C.D. Chen, K.J. Ma, IEEE Trans. Electron. Packag. Manuf. **26**, 141 (2003).

[110] F. Lehmann, G. Richter, T. Borzenko, V. Hock, G. Schmidt, L.W. Molenkamp, Microelectron. Eng. **65**, 327 (2003).

[111] Y. Xia, J.A. Rogers, K.E. Paul, G.M. Whitesides, Chem. Rev. **99**, 1823 (1999).

[112] K. R. Williams, R. S. Muller, J. Microelectromech. Syst. **5**, 256 (1996).

[113] K. R. Williams, K. Gupt, M. Wasilik, J. Microelectromech. Syst. **12**, 761 (2003).

[114] G. S. Oehrlein, Mat. Sci. Eng. B-Solid. **4**, 441 (1989).

[115] M. E. Barone, D. B. Graves, J. Appl. Phys. **78**, 6604 (1995).

[116] S.J. Pearton, Int. J. Mod. Phys. B **08**, 1781 (1994).

[117] J Hopwood, Plasma Sources Sci. Technol. **1**, 109 (1992).

[118] K. Grigoras, S. Franssila, V.-M. Airaksinen, Thin Solid Films **516**, 5551 (2008).

[119] M. D. Henry, S. Walavalkar, A. Homyk, A. Scherer, Nanotechnology **20**, 255305 (2009).

[120] K. Grigoras, L. Sainiemi, J. Tiilikainen, A. Saynatjoki, V.-M. Airaksinen, S. Franssila, J. Phys.: Conf. Ser. **61**, 369 (2007).

[121] J. Yeom, Yan Wu, J. C. Selby, M. A. Shannon, J. Vac. Sci. Technol. B **23**, 2319 (2005).

[122] D. Xia, Z. Ku, S. C. Lee, S. R. J. Brueck, Adv. Mater. **23**, 147 (2011).

[123] Y. Zhao, T. Ikeda, *Smart Light-Responsive Materials: Azobenzene-Containing Polymers and Liquid Crystals* (A John Willey and Sons, Hoboken, NJ, USA 2009).

[124] A. Shishido , Polym. J. **42**, 525 (2010).

[125] N. K. Viswanathan, D. Y. Kim, S. Bian, J. Williams, W. Liu, L. Li, L. Samuelson, J. Kumar, S. K. Tripathy, J. Mater. Chem. **9** , 1941 (1999).

[126] H. Yu, T. Iyoda, T. Ikeda, J. Am. Chem. Soc. **128**, 11010 (2006).

[127] S. Lee, H. S. Kang, J.-K. Park, Adv. Funct. Mater. **21**, 1770 (2011).

[128] S. Lee, Y.-C. Jeong, J.-K. Park, Opt. Express **15**, 14550 (2007).

[129] C. J. Barrett, J. Mamiya, K. G. Yager, T. Ikeda, Soft Matter **3**, 1249 (2007).

[130] A. Natansohn, P. Rochon, Chem. Rev. **102**, 4139 (2002).

[131] P. Rochon, E. Batalla, A. Natansohn, Appl. Phys. Lett. **66**, 136 (1995).

[132] D. Y. Kim, S. K. Tripathy, L. Li, J. Kumar, Appl. Phys. Lett. **66**, 1166 (1995).

[133] R. Walker, H. Audorff, L. Kador, H. W. Schmidt, Adv. Funct. Mater. **19**, 2630 (2009).

[134] O. Kulikovska, L. M. Goldenberg, J. Stumpe, Chem. Mater. **19**, 3343 (2007).

[135] L. M. Goldenberg, L. Kulikovsky, O. Kulikovska, J. Stumpe, J. Mater. Chem. **19**, 6103 (2009).

[136] A. Priimagi, K. Lindfors, M. Kaivola, P. Rochon, ACS Appl. Mater. Interfaces **1**, 1183 (2009).

[137] T. Ubukata, T. Seki, K. Ichimura, Adv. Mater. **12**, 1675 (2000).

[138] M. G. Moharam, T. K. Gaylord, J. Opt. Soc. Am., **72**, 1385 (1982).

[139] S. Lee, J. Shin, Y.-H. Lee, S. Fan, J.-K. Park, Nano Lett. **10**, 296 (2010).

[140] P. Huh, F. Yan, L. Li, M. Kim, R. Mosurkal, L. A. Samuelson, J. Kumar, J. Mater. Chem. **18**, 637 (2008).

[141] A. Priimagi A. Shevchenko, J. Polym. Sci. Part B **52**, 163 (2014).

[142] C. Hubert, C. Fiorini-Debuisschert, I. Maurin, J. M. Nunzi, P. Raimond, Adv. Mater. **14**, 729 (2002).

[143] E. Ishow, R. Camacho-Aguilera, J. Guerin, A. Brosseau, K. Nakatani, Adv. Funct. Mater. **19**, 796 (2009).

[144] J. Yin, G. Ye, X. Wang, Langmuir (26), 6755 (2009).

[145] A. Ambrosio, S. Girardo, A. Camposeo, D. Pisignano, P. Maddalena, Appl. Phys. Lett. **102**, 093102 (2013).

[146] H. Schift, J. Vac. Sci. Technol. B **26**, 458 (2008).

[147] Y. Liang, P. Murphy, W.-D. Li, S. Y Chou, Nanotechnology **20**, 465305 (2009).

[148] T. R. Jensen, G. C. Schatz, R. P. Van Duyne, J. Phys. Chem. B **103**, 2394 (1999).

[149] K. A. Willets, R. P. Van Duyne, Annu. Rev. Phys. Chem. **58**, 267 (2007).

[150] J. Homola, S. S. Yee, G. Gauglitz, Sensor. Actuat. B **54**, 3 (1999).

[151] V. E. Ferry, M. A. Verschuuren, H. B. T. Li, R, E. I. Schropp, H. A. Atwater, A. Polman, Appl. Phys. Lett. **95**, 183503 (2009).

[152] P. Grahn, *Theoretical Description and Design of Optical Nanomaterials* (Aalto University, Helsinki, 2014).

Aalto-DD 116/2015

ISBN 978-952-60-6336-2 (printed)
ISBN 978-952-60-6337-9 (pdf)
ISSN-L 1799-4934
ISSN 1799-4934 (printed)
ISSN 1799-4942 (pdf)

Aalto University
School of Science
Department of Applied Physics
www.aalto.fi

BUSINESS +
ECONOMY

ART +
DESIGN +
ARCHITECTURE

SCIENCE +
TECHNOLOGY

CROSSOVER

DOCTORAL
DISSERTATIONS